Atmos. Chem. Phys., 17, 8837–8865, 2017
https://doi.org/10.5194/acp-17-8837-2017

Atmospheric Chemistry and Physics
Open Access
EGU

Organic carbon at a remote site of the western Mediterranean Basin: sources and chemistry during the ChArMEx SOP2 field experiment

Vincent Michoud[1,2], Jean Sciare[3,4], Stéphane Sauvage[1], Sébastien Dusanter[1,5], Thierry Léonardis[1], Valérie Gros[3], Cerise Kalogridis[3], Nora Zannoni[3], Anaïs Féron[3], Jean-Eudes Petit[3,6,a], Vincent Crenn[3], Dominique Baisnée[3], Roland Sarda-Estève[3], Nicolas Bonnaire[3], Nicolas Marchand[7], H. Langley DeWitt[7], Jorge Pey[7,b], Aurélie Colomb[8], François Gheusi[9], Sonke Szidat[10], Iasonas Stavroulas[4], Agnès Borbon[2,c], and Nadine Locoge[1]

[1]IMT Lille Douai, Univ. Lille, SAGE – Département Sciences de l'Atmosphère et Génie de l'Environnement, 59000 Lille, France
[2]LISA, CNRS UMR7583, Université Paris Est Créteil (UPEC), Université Paris Diderot (UPD), Institut Pierre Simon Laplace (IPSL), Créteil, France
[3]LSCE, IPSL, CEA et Université de Versailles, CNRS, Saint-Quentin, France
[4]The Cyprus Institute, Energy, Environment and Water Research Center, Nicosia, Cyprus
[5]School of Public and Environmental Affairs, Indiana University, Bloomington, IN, USA
[6]INERIS, 60550 Verneuil-en-Halatte, France
[7]Aix Marseille Univ., CNRS, LCE, Marseille, France
[8]LaMP, CNRS UMR6016, Clermont Université, Université Blaise Pascal, Aubière, France
[9]Laboratoire d'Aérologie, Université de Toulouse, CNRS, Toulouse, France
[10]Department of Chemistry and Biochemistry & Oeschger Centre for Climate Change Research, University of Bern, Bern, Switzerland
[a]now at: Air Lorraine, 20 rue Pierre Simon de Laplace, 57070 Metz, France
[b]now at: the Geological Survey of Spain, 50006 Zaragoza, Spain
[c]now at: LaMP, CNRS UMR6016, Clermont Université, Université Blaise Pascal, Aubière, France

Correspondence to: Vincent Michoud (vincent.michoud@lisa.u-pec.fr)
and Stéphane Sauvage (stephane.sauvage@mines-douai.fr)

Received: 26 October 2016 – Discussion started: 23 January 2017
Revised: 16 May 2017 – Accepted: 2 June 2017 – Published: 21 July 2017

Abstract. The ChArMEx (Chemistry and Aerosols Mediterranean Experiments) SOP2 (special observation period 2) field campaign took place from 15 July to 5 August 2013 in the western Mediterranean Basin at Ersa, a remote site in Cape Corse. During the campaign more than 80 volatile organic compounds (VOCs), including oxygenated species, were measured by different online and offline techniques. At the same time, an exhaustive description of the chemical composition of fine aerosols was performed with an aerosol chemical speciation monitor (ACSM). Low levels of anthropogenic VOCs (typically tens to hundreds of parts per trillion for individual species) and black carbon (0.1–0.9 $\mu g\,m^{-3}$) were observed, while significant levels of biogenic species (peaking at the ppb level) were measured. Furthermore, secondary oxygenated VOCs (OVOCs) largely dominated the VOC speciation during the campaign, while organic matter (OM) dominated the aerosol chemical composition, representing 55 % of the total mass of non-refractory PM_1 on average (average of $3.74 \pm 1.80\,\mu g\,m^{-3}$), followed by sulfate (27 %, $1.83 \pm 1.06\,\mu g\,m^{-3}$), ammonium (13 %, $0.90 \pm 0.55\,\mu g\,m^{-3}$) and nitrate (5 %, $0.31 \pm 0.18\,\mu g\,m^{-3}$).

Positive matrix factorization (PMF) and concentration field (CF) analyses were performed on a database containing 42 VOCs (or grouped VOCs), including OVOCs, to iden-

tify the covariation factors of compounds that are representative of primary emissions or chemical transformation processes. A six-factor solution was found for the PMF analysis, including a primary and secondary biogenic factor correlated with temperature and exhibiting a clear diurnal profile. In addition, three anthropogenic factors characterized by compounds with various lifetimes and/or sources have been identified (long-lived, medium-lived and short-lived anthropogenic factors). The anthropogenic nature of these factors was confirmed by the CF analysis, which identified potential source areas known for intense anthropogenic emissions (north of Italy and southeast of France). Finally, a factor characterized by OVOCs of both biogenic and anthropogenic origin was found. This factor was well correlated with submicron organic aerosol (OA) measured by an aerosol chemical speciation monitor (ACSM), highlighting the close link between OVOCs and organic aerosols; the latter is mainly associated (96 %) with the secondary OA fraction. The source apportionment of OA measured by ACSM led to a three-factor solution identified as hydrogen-like OA (HOA), semi-volatile oxygenated OA (SV-OOA) and low volatility OOA (LV-OOA) for averaged mass concentrations of 0.13, 1.59 and 1.92 $\mu g\,m^{-3}$, respectively.

A combined analysis of gaseous PMF factors with inorganic and organic fractions of aerosols helped distinguish between anthropogenic continental and biogenic influences on the aerosol- and gas-phase compositions.

1 Introduction

Organic matter is directly emitted into the atmosphere both in the gas phase as volatile organic compounds (VOCs) and in the aerosol phase as primary organic aerosol (POA). The sources can be of biogenic (from land or marine ecosystems) or anthropogenic (from traffic, industrial activities or residential heating) origins. Once emitted, it can be transported over long distances and undergo chemical transformations due to atmospheric photo-oxidants, such as ozone (O_3), the hydroxyl radical (OH) or the nitrate radical (NO_3) at night. The hydroxyl radical is the main oxidant in the atmosphere and therefore controls the fate of most VOCs through oxidation cycles that lead to the formation of tropospheric O_3 (Seinfeld and Pandis, 1998) and a large number of secondary oxygenated VOCs (OVOCs; Atkinson, 2000; Goldstein and Galbally, 2007). OVOCs subsequently react with atmospheric oxidants, leading to multifunctionalized compounds of lower volatility through a multigenerational oxidation process (Kroll and Seinfeld, 2008; Jimenez et al., 2009; Aumont et al., 2012). These semi-volatile compounds take part in the formation of secondary organic aerosols (SOAs) through condensation onto preexisting particles (Kanakidou et al., 2005). Organic aerosols are of particular interest owing to their impact on human health (Pope and Dockery, 2006) and their direct (Forster et al., 2007) or indirect (Lohmann and Feichter, 2005) effect on the earth's climate. Furthermore, chemical models suggest that the secondary organic gaseous fraction, still reactive and multifunctionalized several days after emission, can be transported over long distances, affecting the oxidant budget and the formation of ozone and SOA at remote locations (Aumont et al., 2005; Madronich, 2006). It is therefore essential to understand the sources and fate of organic matter in the atmosphere, especially its evolution during long-range transport.

Positive matrix factorization (PMF) models (Paatero and Tapper, 1994; Paatero, 1997) have been widely used to identify and quantify sources of VOCs, generally in urban environments (e.g., Latella et al., 2005; Leuchner and Rappenglück, 2010; Gaimoz et al., 2011; Yuan et al., 2012). This type of analysis allows for the separation of different sources (e.g., vehicular exhaust, fuel evaporation and residential heating) and the apportionment of those sources to the VOC budget. PMF was also used at remote sites (Lanz et al., 2009; Sauvage et al., 2009; Leuchner et al., 2015), despite the need to assume mass conservation between the source location and the measurement site in this approach (Hopke, 2003). In such environments, PMF can be used as a tool to identify aged primary sources and the photochemical formation of organic trace gases. This approach can therefore be useful to gain insight into the sources and processes involved in the evolution of organic trace gases measured at remote locations. For example, Leuchner et al. (2015) applied PMF to 24 C_2–C_8 non-methane hydrocarbons (NMHCs) measured at a remote site at Hohenpeissenberg (980 m a.s.l.). The authors obtained six different factors assigned to primary biogenic emissions, short-lived combustion, short- and long-lived evaporative emissions, residential heating and a background component.

Similar PMF approaches have also been conducted on the organic fraction of aerosols measured mostly by an aerosol mass spectrometer (AMS) to identify different components characterized by their sources, their formation and/or their chemical composition (Ng et al., 2010a; Zhang et al., 2011). For example, aerosol factors such as HOA (hydrocarbon-like organic aerosol), and OOA (oxygenated-like organic aerosol) are commonly extracted from AMS spectra using PMF analysis and are attributed to POA and SOA, respectively (Zhang et al., 2011). The latter can also be separated into several factors as a function of volatility: low volatility OOA (LV-OOA) and semi-volatile OOA (SV-OOA) (Zhang et al., 2011). For example, Hildebrandt et al. (2010) detected two types of OOA with low volatility using PMF on AMS data recorded at Finokalia, an eastern Mediterranean remote site; no HOA was present in detectable amounts. In contrast, PMF analysis applied to aerosol measurements taken at an urban background site in Barcelona in spring, in the western Mediterranean Basin, revealed a significant impact by local primary emissions from HOA, cooking organic aerosol (COA) and biomass burning organic aerosol (BBOA) factors accounting

for 44 % of OA; regional and local secondary sources (LV-OOA and SV-OOA) dominated the OA burden (Mohr et al., 2012). Another study combining ACSM measurements and ^{14}C analysis was conducted in Barcelona in summer 2013. The results revealed a large contribution of anthropogenic sources for this environment with fossil OC representing 46 to 57 % of total OA. However, a larger contribution of secondary origin for fossil OC (> 70 %) and nonfossil OC (37–60 %) was observed, leading to a large fraction of OA contained in OOA factors (Minguillón et al., 2016). Macro-tracer analysis represents an alternative solution to apportioning OA and can be used to allocate and verify specific OA factors derived from PMF analysis. For instance, in atmospheres not impacted by biomass burning, water-soluble organic compounds (WSOC) have been shown to provide valuable information on SOA that could be mainly of biogenic origin (Sullivan et al., 2004, 2006; Heald et al., 2006; Miyazaki et al., 2006; Kondo et al., 2007; Weber et al., 2007; Hennigan et al., 2008b).

More recently, combined source apportionments of organic aerosol and VOCs were performed in urban environments (Slowik et al., 2010; Crippa et al., 2013a), allowing a better classification of organic aerosol (OA) from the PMF analysis. This type of analysis also provided insight into OA sources, such as the identification of gaseous precursors.

Residential time analysis identifies the geographical location of potential source areas by combining measured or estimated variables at a receptor site with back-trajectory analyses (Ashbaugh et al., 1985; Seibert et al., 1994; Stohl, 1996). Combined with PMF results, these models have been used to locate source regions of PMF factors (Hwang and Hopke, 2007; Lanz et al., 2009; Tian et al., 2013). This association of receptor-oriented models can be powerful in identifying the nature of the source or the chemical processes characterizing PMF factors. The concentration field (CF) is one of these source-receptor inverse models, which was developed by Seibert et al. (1994). It consists of a redistribution of the measured or estimated variables in grid cells along estimated back trajectories.

The Mediterranean Basin is an ideal location to study the sources and the fate of organic carbon during long-range transport since it is impacted by strong natural and anthropogenic emissions and undergoes intense photochemical events (Lelieveld et al., 2002). The ChArMEx project (Chemistry and Aerosols Mediterranean Experiments) aims at assessing the present and future state of the atmospheric environment and its impacts in the Mediterranean Basin. This initiative proposes setting up a coordinated experimental effort for an assessment of the regional budgets of tropospheric trace species, their trends and their impacts on air quality, marine biogeochemistry and regional climate. For that purpose an intensive field campaign was performed during summer 2013 at Cape Corse (north of the island of Corsica) where a full suite of trace gases and aerosol species were measured for 3 weeks. In the framework of ChArMEx, the CARBO-SOR (CARBOn within continental pollution plumes: SOurces and Reactivity) project aimed more specifically at investigating the sources of primary and secondary organic trace gases and the composition of continental plumes reaching Cape Corse, with the goal of assessing their impacts on the photo-oxidants and/or SOA sources and levels.

As part of the ChArMEx and CARBO-SOR projects, this study investigates the sources and the chemistry of atmospheric organic matter by combining different statistical tools, i.e., the PMF and ME-2 (multilinear engine-2) models and the concentration field method. This approach was used to (i) identify the covariation factors of measured VOCs that are representative of primary emissions at various stages of aging and chemical transformation occurring during long-range transport and to (ii) better characterize the different fractions of organic aerosol. The PMF factors were then used to assess the origin of non-refractive organic species in PM_1 (particulate matter with an aerodynamic diameter below 1 µm) observed at the measurement site, especially to try to determine the fraction of biogenic versus anthropogenic OA.

2 The ChArMEx SOP2 ground-based field experiment

2.1 Description of the Cape Corse ground site

The ChArMEx SOP2 (short observation period 2) field campaign took place from 15 July to 5 August 2013. The measurement site is located in Ersa at Cape Corse (42.969° N, 9.380° E) at the top of a hill (533 m a.s.l.; meters above sea level) a few kilometers from the sea in all directions (6, 4.5 and 2.5 km from the east, north and west sides, respectively; see Fig. 1). The measurement site is surrounded by widespread vegetation, such as the "maquis" shrubland typical of Mediterranean areas (Zannoni et al., 2015). The closest city, Bastia, is located approximately 30 km south of the site. It is the second largest city in Corsica (44 121 inhabitants; census 2012), which hosts the main harbor of the island with about 413 000 and 614 000 passengers in July and August 2013, respectively (CCI Territorial Bastia Haute Corse, 2013). However, the Cape Corse peninsula is characterized by a mountain range (peaking between 1000 and 1500 m a.s.l.), which acts as a natural barrier isolating the measurement site from any atmospheric flow originating from Bastia.

2.2 VOC measurements

During the ChArMEx SOP2 field campaign, more than 80 VOCs, including non-methane hydrocarbons (NMHCs) and oxygenated (O) VOCs, were measured using complementary online and offline techniques with sampling inlets located approximately 1.5 m above the roof of a trailer in which the instruments were housed. Table 1 summarizes the VOC measurements performed during the campaign.

Table 1. Summary of VOC measurements performed at Cape Corse during the ChArMEx SOP2 field campaign. DL is detection limit.

Instrument	Time resolution	# species	# species > DL	Overall uncertainties (%)	DL range (ppt)	Examples	Mean ± 1σ (ppt)	DL (ppt)
PTR-TOF-MS	10 min	16	16	6–23	7–500	isoprene	194 ± 224	20
						sum terpenes	407 ± 462	15
						acetaldehyde	329 ± 118	50
						acetic acid	1152 ± 405	110
Online GC-FID-FID	90 min	43 NMHC	22	5–23	10–100	ethane	891 ± 187	50
						butane	65 ± 92	20
						propene	31 ± 13	10
						ethyne	92 ± 49	20
						benzene	27 ± 12	10
						toluene	77 ± 65	20
Online GC-FID-MS	90 min	16 OVOCs C_3–C_7 6 NMHCS	22	5–14	5–100	α-pinene	108 ± 77	10
						β-Pinene	141 ± 124	10
						limonene	31 ± 35	10
						ethanol	184 ± 79	20
						hexanal	101 ± 50	20
Offline solid adsorbents	180 min	35 NMHCs C_5–C_{16} 5 C_6–C_{12} *n*-aldehydes	28	∼ 25	∼ 5	nonane	8 ± 46	5
						decane	3 ± 3	5
						styrene	6 ± 5	5
						hexanal	17 ± 13	5
Offline DNPH	180 min	16 C_1–C_8	14	∼ 25	6–40	formaldehyde	2483 ± 868	40
						acetone	3430 ± 1126	20
						MEK	481 ± 385	20
						MACR	59 ± 35	15
						GLY	146 ± 81	15

Figure 1. Localization and geographical configuration of the measurement site in Ersa at Cape Corse (source: Google Maps). The white solid square in the insert (top left) represents the localization of the city of Bastia.

Sixteen protonated masses were extracted from a proton transfer reaction time-of-flight mass spectrometer (PTR-TOF-MS; KORE Technology®, second generation), leading to the measurements of OVOCs (alcohols, such as methanol m/z 33.03, aldehydes, ketones and carboxylic acids), aromatics (sum of both C–8 and C–9 aromatics; m/z 107.09 and 121.10, respectively) and biogenic VOCs (BVOCs, such as isoprene, m/z 69.07, and the sum of monoterpenes, m/z 137.13). Ambient air was sampled through a 5 m long PFA line (perfluoroalkoxy, 1/4″ OD) held at 50 °C using a constant flow rate of 1.2 L min^{-1} to minimize the residence time to 4 s. The PTR-TOF-MS sampling flow rate was set at 150 mL min^{-1} and an additional pump was used to raise the flow rate to the required 1.2 L min^{-1} in the sampling line. The instrument was operated at a reactor pressure and temperature of 1.33 mbar and 40 °C, respectively, leading to an E/N ratio of 135 Td.

An automated zero procedure was performed every hour for 10 min. Humid zero air was generated by passing ambient air through a catalytic converter (stainless steel tubing filled with Pt wool held at 350 °C) allowing for the same relative humidity as in the ambient air. During the campaign, the PTR-TOF-MS was calibrated every 3 days using a gas calibration unit (Ionicon®) and various standards, including a mix of 15 VOCs (NMHCs, OVOCs and chlorinated VOCs) in a canister (Restek®), a mix of 9 NMHCs in a second cylinder (Praxair®) and a mix of 9 OVOCs in a cylinder (Praxair®; see Table S1 in the Supplement). Additional calibrations were performed before and after the campaign using permeation tubes (Kin-Tek Analytical®) for carboxylic acids and a liquid calibration unit (Ionicon®) with a certified solution for methyl glyoxal. To account for a possible drift of the PTR-TOF-MS sensitivity during the campaign, relative calibration factors were determined for the carboxylic acids and methyl glyoxal using a specific VOC as a reference (present in the standard mixtures used to calibrate the PTR-TOF-MS during the campaign with an m/z value as close as possible for each

compound; e.g., acetaldehyde, acetone and methyl ethyl ketone for formic acid, acetic acid and methyl glyoxal, respectively).

The signal of every unit mass is accumulated over 10 min and normalized by the signals of H_3O^+ and the first water cluster $H_3O^+(H_2O)$ as proposed by de Gouw and Warneke (2007). Concentrations are calculated using Eq. (1):

$$[X] = \frac{i_{\mathrm{X\_net}}}{\left(i_{\mathrm{H_3O^+}} + X_\mathrm{r} \cdot i_{\mathrm{H_3O^+(H_2O)}}\right)} \cdot \frac{150000}{R_{f,X}}, \quad (1)$$

where $[X]$ represents the mixing ratio of a given VOC, $i_{\mathrm{X\_net}}$ is the net signal recorded for this VOC and $i_{\mathrm{H_3O^+}}$ and $i_{\mathrm{H_3O^+(H_2O)}}$ are the signals of H_3O^+ and $H_3O^+(H_2O)$ at m/z 19 and 37 respectively recorded at m/z 21 and 39 to avoid any saturation of the detector at m/z 19 and 37 and recalculated using the isotopic ratio between ^{16}O and ^{18}O. X_r is a factor introduced to account for the effect of humidity on the PTR-TOF-MS sensitivity (de Gouw and Warneke, 2007) and determined experimentally through calibrations performed at various relative humidities. $R_{f,X}$ is the sensitivity determined during calibration experiments (in ncts ppt^{-1}) and normalized to 150 000 counts s^{-1} of H_3O^+ ions. The latter is the number of counts of reagent ions observed in our PTR-TOF-MS instrument.

Forty-three C_2–C_{12} NMHCs, including alkanes, alkenes, alkynes and aromatics, were measured using an online gas chromatograph (GC) equipped with two columns and a dual flame ionization detection (FID-FID) system (Perkin Elmer®). This instrument has been previously described in detail by Badol et al. (2004). Air is sampled via a 5 m PFA line (1/8″ OD) at a flow rate of 15 mL min^{-1}. Ambient air passes through a Nafion membrane to dry it and is then preconcentrated for 40 min onto a sorbent trap made of Carbopack B and Carbosieve SIII and held at −30 °C by a Peltier cooling system. The trap is then heated to 300 °C (40 °C s^{-1}) to desorb and inject VOCs in a Perkin Elmer GC system. The chromatographic separation is performed using two capillary columns with a switching facility. This approach allows for a better separation and reduces co-elution issues (Badol et al., 2004). The first column designed for C_6–C_{12} compounds is a CP-Sil 5 CB (50 m × 0.25 mm × 1 µm), while the second column designed for the C_2–C_5 compounds is a plot Al_2O_3/Na_2SO_4 (50 m × 0.32 mm × 5 µm). The separation step lasts 50 min, leading to a total time of 1 h 30 min. Finally, eluted compounds are detected using the two FID detectors. Calibrations were performed at the beginning, middle and end of the campaign using a standard mixture containing 32 compounds (NPL®; see Table S2).

Sixteen C_3–C_7 OVOCs, including aldehydes, ketones, alcohols, ethers, esters and six NMHCs, including BVOCs and aromatics, were measured using an online GC-FID mass spectrometer (MS). This instrument has been described in detail by Roukos et al. (2009). Ambient air is sampled via a 5 m PFA line (1/8″) at a flow rate of 15 mL min^{-1} by an air server unit (Markes International®; Unity 1) and passes through a KI ozone scrubber. The sampled air is pre-diluted (50 % dilution) with dry zero air to keep the relative humidity below 50 %. A sample is then collected into an internal trap cooled by a Peltier system at 12.5 °C and consists of a 1.9 mm i.d. quartz tube filled with two different sorbents (5 mg of Carbopack B and 75 mg of Carbopack X; Supelco®). Compounds trapped onto the sorbents are then thermally desorbed at 280 °C and injected into the column and analyzed by a GC (Agilent®) equipped with an FID for quantification and a mass spectrometer (MS) to help with the identification. The thermally desorbed compounds are passed through a highly polar CP-lowox column (30 m × 0.53 mm × 10 µm; Varian®) for separation. The sampling and analysis steps last 40 and 50 min, respectively, for a total time of 1 h 30 min. Calibrations were performed several times during the campaign using a standard mixture containing 29 compounds (Praxair®; see Table S2).

Thirty-five C_5–C_{16} NMHCs, including alkanes, alkenes, aromatics and BVOCs, as well as five C_6–C_{12} *n*-aldehydes were collected by active sampling into sorbent cartridges using an automatic clean room sampling system (Tera Environment®) and later analyzed by GC-FID. This technique has already been described by Detournay et al. (2011) and its setup in the field was discussed by Ait-Helal et al. (2014). Air was sampled via a 3 m PFA line (1/4″ OD) at 200 mL min^{-1} and passed through an MnO_2 ozone scrubber and a stainless steel particle filter (2 µm pore size diameter). VOCs are collected over 3 h in cartridges filled with Carbopack C (200 mg) and Carbopack B (200 mg), formerly conditioned with purified air at 250 °C over 24 h.

Finally, sixteen C_1–C_8 carbonyl compounds were collected offline over 3 h using the same sampling device as for solid sorbent cartridges by active sampling on dinitrophenylhydrazine (DNPH) cartridges (Waters®). These compounds were later analyzed by high-performance liquid chromatography (HPLC) with UV detection. Air was sampled via a 3 m PFA line (1/4″ OD) at 1.5 L min^{-1} and passed through a KI ozone scrubber and a stainless steel particle filter (2 µm pore size diameter). Data are available only for the first 10 days of the campaign (15–25 July) due to unresolved leakage issues for the rest of the campaign; hence contamination of the cartridges with indoor air from the trailer was suspected.

The detection limits for each species measured by all five techniques were determined as 3σ of the blank variation for PTR-TOF-MS and offline sampling methods and as 3σ of the baseline fluctuations for online GCs. The uncertainties for each species were estimated following the "Aerosols, Clouds, and Trace gases Research InfraStructure network" (ACTRIS) guidelines for uncertainty evaluation (ACTRIS Measurement Guideline VOC, 2014) taking into account precision, detection limits and systematic errors in the measurements. The range of uncertainties and detection limits for each technique are given in Table 1. Furthermore, systematic intercomparisons for compounds measured by different techniques

(e.g., isoprene, monoterpenes, acetone, *n*-pentane and benzene) were performed to validate the database (not shown).

2.3 Ancillary gas measurements

During the campaign, measurements of other trace gases (NO, NO_2, O_3, CO, CO_2, CH_4, H_2O and SO_2) were additionally performed at the same measurement site.

NO and NO_2 were measured by a commercial analyzer (Cranox II; Eco Physics®) using ozone chemiluminescence with a time resolution of 5 min. Since this technique allows for the direct measurement of NO only, NO_2 was converted into NO using a photolytic converter incorporated in the analyzer.

O_3 was measured using a UV absorption analyzer (TEI 49i; Thermo Environmental Instruments Inc®) at a time resolution of 5 min. CO, CO_2, CH_4 and H_2O were simultaneously measured by a commercial analyzer (G2401; Picarro®) based on cavity ring-down spectroscopy (CRDS). Finally, SO_2 was measured by a commercial analyzer (TEI 43i; Thermo Environmental Instruments Inc®) using fluorescence spectroscopy at a time resolution of 5 min.

2.4 Aerosol measurements

Online measurements of organic aerosols (PILS-IC, PILS-TOC, OCEC Sunset field instruments and Q-ACSM) have been available since the beginning of June 2013, but the data reported here are restricted to the ChArMEx SOP2 period (15 July to 5 August 2013) for which VOC measurements have been performed.

In addition, black carbon (BC) was continuously monitored during the same extended period using a seven-wavelength Aethalometer (model AE-31; Magee Scientific®) at a time resolution of 15 min.

2.4.1 PILS-IC instrument

Measurements of major anions (Cl^-, NO_3^- and SO_4^{2-}), cations (Na^+, NH_4^+, K^+, Mg^{2+} and Ca^{2+}) and light organics (methanesulfonate, MSA; oxalate) in PM_{10} were performed using a particle-into-liquid-sampler (PILS; Orsini et al., 2003) running at $11.8 \pm 0.5\,L\,min^{-1}$ and coupled with two ion chromatographs (ICs). More details on the settings of the PILS-IC can be found in Sciare et al. (2011). During this field campaign, ambient concentrations of ions were corrected from blanks performed every day for 1 h and achieved by placing a total filter upstream of the sampling system. Very low blank values (typically below 1 ppb) were systematically detected for all ions, providing further confidence in the efficiency of the acidic or basic denuders set upstream of the PILS, the lack of contaminants in our system and the quality of our Milli-Q water for the duration of the study. Liquid flow rates of the PILS were delivered by peristaltic pumps and set to $1.0\,mL\,min^{-1}$ for producing steam inside the PILS and $0.37 \pm 0.02\,mL\,min^{-1}$ for rinsing the impactor. Calibrations (five to seven points) of anions and cations (including light organics) were performed every 2 weeks (from the end of May 2013 to the beginning of August 2013) with no significant drift reported (e.g., below 5 % difference on average). Based on IC settings, the detection limit (2σ) for ions was typically 0.1 ppb, which corresponds to an atmospheric concentration of $\sim 1\,ng\,m^{-3}$. The overall uncertainty associated with PILS-IC measurements includes variability in air sampling flow rate, liquid flow rate, calibration and collection efficiency and was estimated to be on the order of 25 %. Time resolutions were typically 24 min for anions (including light organics) and 12 min for cations. Because this study focuses on organics in the atmosphere, only MSA and oxalate data will be presented and discussed here. A total of 761 and 996 valid data points for MSA and oxalate were obtained, respectively, with concentrations ranging from 4 to $59\,ng\,m^{-3}$ for MSA ($21\,ng\,m^{-3}$ on average) and from 1 to $24\,ng\,m^{-3}$ for oxalate ($10\,ng\,m^{-3}$ on average).

2.4.2 PILS-TOC instrument

Measurements of water-soluble organic compounds (WSOCs) in PM_1 were performed every 4 min using a modified particle-into-liquid-sampler (Brechtel Manufacturing Inc., USA; Sorooshian et al., 2006) coupled with a total organic carbon analyzer (TOC; model Sievers 900; Ionics Ltd, USA). More information on the operating procedure of this instrument is provided by Sciare et al. (2011). The PILS-TOC instrument runs at $15\,L\,min^{-1}$, and a measured dilution factor of 1.30 was taken for the instrument, which is close that reported by Sullivan et al. (2006). A polyethylene filter with a 0.45 µm pore size diameter was set in-line in the aerosol liquid flow (downstream of the PILS collector) in order to analyze solely the water-soluble OC fraction. Daily blanks for the PILS-TOC instrument were achieved by placing a total filter upstream of the sampling system for 1h. In this configuration, it took approximately 15 min to reach blank values that were very stable during the campaign, showing a mean concentration of 35.6 ± 2.6 ppbC, which is very similar to that reported by Sciare et al. (2011). Note that most of the blank concentration refers to the TOC concentration in the ultra-pure water used in the PILS instrument (typically 25 ppbC), suggesting little contamination in the PILS instrument and good efficiency of the VOC denuder placed upstream. Also note that the daily blanks for the PILS-TOC instrument were performed at different hours of the day and did not show a clear diurnal pattern that could be linked to diurnal variations in VOCs. Ambient WSOC measurements were then corrected from this blank value. The limit of quantification for ambient WSOC measurements was estimated as 2σ (twice the uncertainty calculated for the blank concentrations), corresponding to about $0.48\,\mu gC\,m^{-3}$. A total of 6592 valid data points were collected during the period of the study (15 July to 5 August 2013), corresponding to a mean ambient

(blank corrected) WSOC concentration of 11.6 ± 6.7 ppbC (i.e., $1.00 \pm 0.60\,\mu gC\,m^{-3}$).

2.4.3 OCEC Sunset field instrument

Semicontinuous (2 h time resolution) concentrations of elemental carbon (EC) and organic carbon (OC) in $PM_{2.5}$ were obtained in the field from an OCEC Sunset field instrument (Sunset Laboratory, Forest Grove, OR, USA; Bae et al., 2004) running at $8\,L\,min^{-1}$. A denuder provided by the manufacturer was set upstream in order to remove possible adsorption of VOCs from the filter used to collect fine aerosols in the instrument. The measurement uncertainty given by the OCEC Sunset field instrument is poorly described in the literature and an estimate of 20 % for this uncertainty was taken here following Peltier et al. (2007). This instrument ran continuously for the duration of the campaign (15 July to 5 August 2013) with 252 valid EC and OC data points obtained.

These online EC and OC measurements were also intercompared with an analysis from an offline filter sampling to check their reliability, leading to satisfactory agreement between the two methods (see Fig. S3a in the Supplement). EC online measurements were also compared to BC measurements from an Aethalometer, leading to satisfactory agreement (see Fig. S3b).

2.4.4 Q-ACSM instrument

Since summer 2012, measurements of the chemical composition of non-refractory submicron aerosol (NR-PM_1) have been carried out at the measurement site using a quadrupole aerosol chemical speciation monitor (Q-ACSM; Aerodyne Research Inc., Billerica, MA, USA). This recently developed instrument shares the same general structure with the aerosol mass spectrometer (AMS) but has been specifically developed for long-term monitoring. An exhaustive description of ACSM is available in Ng et al. (2011), and a growing number of studies have already reported long-term observations of NR-PM_1 composition and concentrations using it (Ripoll et al., 2015; Minguillón et al., 2015; Petit et al., 2015; Parworth et al., 2015; Budisulistiorini et al., 2015).

The Q-ACSM used here participated in the large intercomparison study of 13 Q-ACSMs that took place at the ACMCC (Aerosol Chemical Monitor Calibration Centre; https://acmcc.lsce.ipsl.fr/) 3 months after this field campaign. For atmospheric concentrations and fragmentation pattern, it showed very good results in terms of reproducibility and consistency (Crenn et al., 2015). Source apportionment performed with the same Q-ACSM (during the intercomparison study at the ACMCC) has also led to very consistent and comparable results (Frölich et al., 2015). The calibration of this instrument with monodispersed (300 nm diameter) ammonium nitrate particles was performed at the ACMCC in May 2013 about 2 months before the start of this study. Because ambient air was dried by a Nafion membrane before entering the Q-ACSM and because ammonium nitrate was not significant during the field campaign, we have kept a constant collection efficiency (CE) of 0.5. On-site atmospheric concentrations delivered by the Q-ACSM were consistent for NR-PM_1 and SO_4 concentrations obtained with colocated online instruments (scanning mobility particle sizer and a particle-into-liquid-sampler ion chromatograph; see Fig. S3c). The Q-ACSM operated continuously for the duration of the campaign (15 July to 5 August 2013) with a total of 1148 valid data points, each with a time resolution of 30 min.

2.5 Back-trajectory classification

A study of back trajectories was performed to identify and classify the origin and typology of the different air masses reaching Cape Corse during the campaign and to support interpretation of the results. Back trajectories of 48 h were calculated every 6 h during the whole campaign with an ending point at the measurement site (42.969° N, 9.380° E; 600 m a.s.l.) using the online version of the HYSPLIT model (HYbrid Single-Particle Lagrangian Integrated Trajectory) developed by the National Oceanic and Atmosphere Administration (NOAA) Air Resources Laboratory (ARL; Draxler and Hess, 1998; Stein et al., 2015). This model was chosen for its easy and quick visualization facility.

A visual classification of these back trajectories was performed as a function of their origin, altitude and wind speed and segregated into five clusters (Fig. 2). A description of the five clusters is provided in Table 2. Four clusters correspond to different wind sectors defined by the origin of the air masses reaching the measurement site (west, northeast, south and northwest). These clusters are characterized by different transit times since the last potential anthropogenic contamination (i.e., since the air mass left the continental coasts). The air masses from the "marine west" cluster have spent 36 to more than 48 h above the sea, while they have spent 10–20 and 12–18 h for the "Europe northeast" and the "France northwest" clusters, respectively (Table 2). For the "Corsica south" cluster, the indicated transit time (12–24 h) considers the time spent by air masses above land (the islands of Corsica and Sardinia) before passing over the sea. These different transit times potentially indicate different atmospheric processing times for the air masses, the longest being for the "marine west" cluster.

The last cluster gathers air masses transported over short distances over 48 h and therefore during calm situations with low wind speeds (Fig. 2). The "calm low wind" cluster and the "marine west" cluster are the two most representative clusters, each representing 30 % of the air mass origin. They are followed by the "Europe northeast" cluster representing 26 %, and then by the "Corsica south" and "France northwest" clusters representing 8 and 6 % of the air mass origins, respectively.

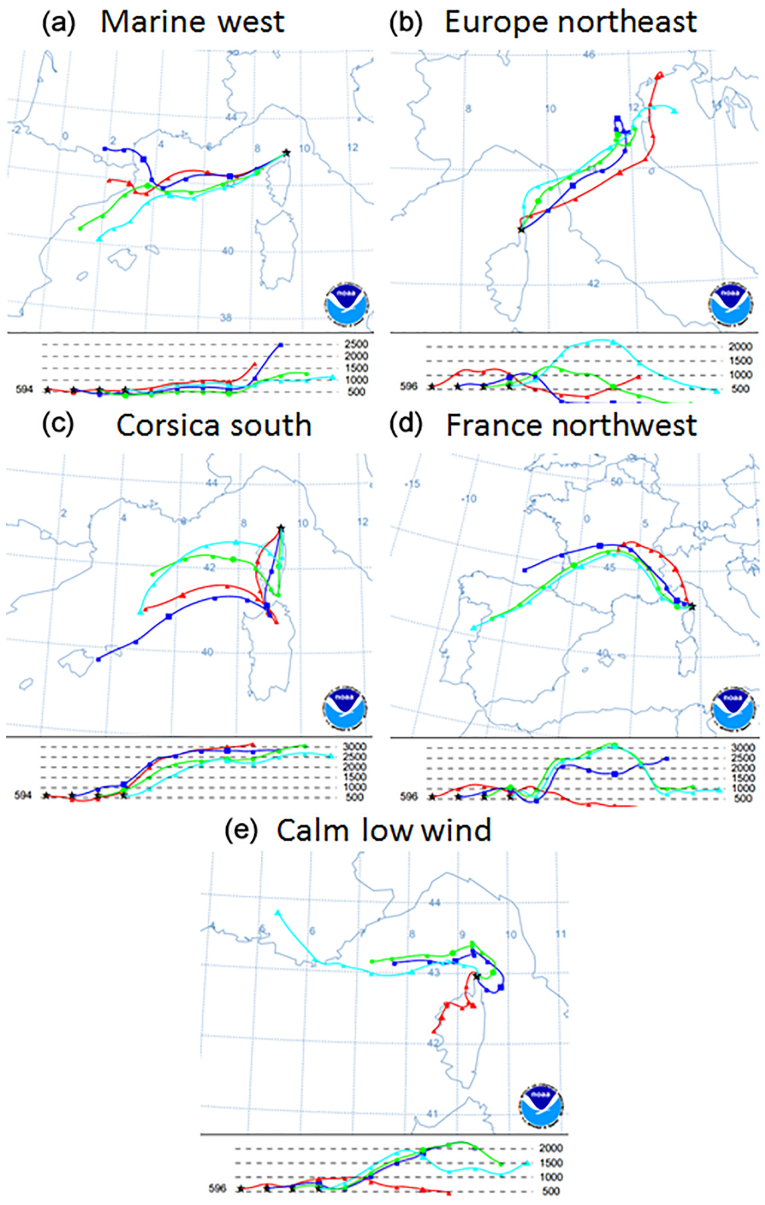

Figure 2. Five back-trajectory clusters identified for the ChArMEx SOP2 field campaign at Cape Corse. This classification was conducted using back trajectories calculated by the HYSPLIT model (NOAA-ARL). The five clusters are illustrated by example maps for four trajectories (interval of 6 h between each; time of arrival indicated by different colors of trajectory) for five single days representative of an isolated cluster (25, 21, 28, 30 and 18 July for marine west, Europe northeast, Corsica south, France west and calm low wind, respectively).

2.6 Photochemical age of air masses

Regarding the relatively long transit time of air masses traveling from continental source areas to the measurement site (from 10 to more than 48 h; see Sect. 2.5), an assessment of the photochemical age using field observations can be performed with specific ratios of long-lived VOCs measured at significant levels at the site. The use of graphic representations of the ratios for three different alkanes, such as ln(butane / ethane) versus ln(propane / ethane), is well suited to assessing the photochemical age of air masses that experienced long-range transport (Rudolph and Johnen, 1990; Jobson et al., 1994; Parrish et al., 2007). Considering an air parcel isolated from any new emissions or mixing with other air parcels and also considering that the main loss of alkanes is their oxidation by the OH radical, the relation of the three alkanes can be estimated as described by Eq. (2) (Jobson et al., 1994):

$$\ln\frac{[\text{butane}]}{[\text{ethane}]} = \frac{k_{\text{butane}} - k_{\text{ethane}}}{k_{\text{propane}} - k_{\text{ethane}}} \ln\frac{[\text{propane}]}{[\text{ethane}]} + \beta, \qquad (2)$$

Table 2. Back-trajectory clusters for the ChArMEx SOP2 field campaign in Cape Corse. The averaged transport time corresponds to the time spent since the last anthropogenic contamination, i.e., since the air masses left the continental coasts.

Clusters	Source region	Averaged transport time	Contribution (%)
Marine West	South France Northeast Spain	36–> 48 h	30 %
Europe northeast	North Italy	10–20 h	26 %
Corsica south	Corsica, Sardinia	12–24 h*	8 %
France northwest	Southeast France	12–18 h	6 %
Calm low wind	Local	Not applicable	30 %

* For the Corsica south cluster, the transport time corresponds to the time spent by the air masses above land (the islands of Corsica and Sardinia) before flying over the sea.

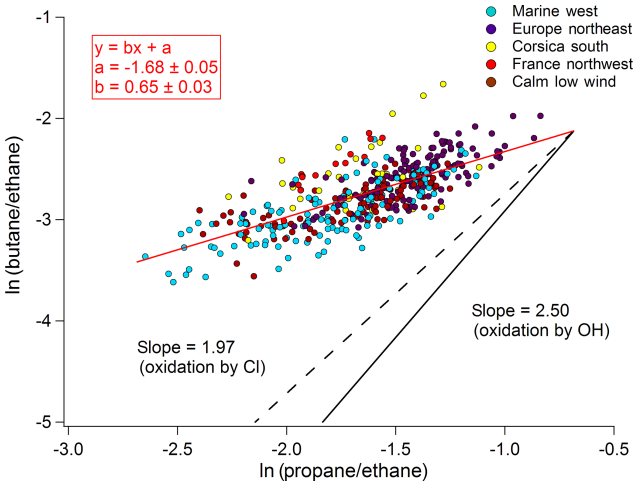

Figure 3. Evolution of ln(butane / ethane) as a function of ln(propane / ethane) during the ChArMEx SOP2 field campaign. The data were color coded as a function of the back-trajectory clusters (light blue, purple, yellow, red and brown for the marine west, Europe northeast, Corsica south, France northwest and calm low wind clusters, respectively). The red line corresponds to the linear regression. The black lines correspond to the theoretical kinetic evolution of the ratios of alkanes due to oxidation by OH only (solid line) or Cl only (dashed line).

where k_i is the bimolecular reaction rate constant of the reaction between the species i and OH. The β parameter depends on the emission ratios of these three species and the reaction rate constants.

Since ethane is the least reactive of these compounds, the ratios will tend to decrease with increasing photochemical age. The evolution of ln(butane / ethane) as a function of ln(propane / ethane) during the ChArMEx SOP2 field campaign in Cape Corse is presented in Fig. 3. The points in Fig. 3 have been color coded as a function of the back-trajectory clusters described in the previous section.

Figure 3 reveals that the air masses of the marine west (light blue) cluster present higher photochemical ages (lower alkane ratios) relative to the air masses of the Europe northeast (purple) cluster, which is consistent with the analysis of back trajectories (Sect. 2.5). Moreover, the good linearity observed in the evolution of the ratios allows for a qualitative comparison of the photochemical age of air masses from the different wind clusters.

These ratios have been compared to ratios observed at measurement sites of different types (see Fig. S4). The ratios obtained during the campaign cover a large range of values with particularly low values for the marine west cluster, which is typical of relatively aged air masses sampled at very remote sites. It indicates that air masses can spend several days over the sea before reaching the measurement site, especially for the marine west cluster. In general, ratios representative of remote locations are observed all along the campaign, confirming the remote nature of the Cape Corse station.

It is noteworthy that the slope observed for our dataset (0.65; see Fig. 3) is significantly lower than the theoretical ones calculated for an isolated air mass experiencing selective oxidation by OH (2.50) or Cl (1.97). The lack of concordance with theoretical slopes has often been observed (e.g., Parrish et al., 1992; McKeen et al., 1996) and has been attributed to the mixing between air parcels of different histories and origins during long-range transport (Parrish et al., 2007 and references therein). A deviation from the theoretical slope could also occur if the sampled air masses were enriched in new emissions from different sources, such as ship or marine emissions, during transport.

3 Source-receptor models

3.1 The positive matrix factorization (PMF)

In this study, US EPA PMF 3.0 was used to perform the factor analysis. For a detailed presentation of the PMF principle, the reader can refer to the first description made by Paatero and Tapper (1994) and to the user guide written by Hopke (2000). A specific dataset at a receptor site can be viewed as a data matrix **X** containing i samples and j measured chemical species. The PMF identifies the number of factors p, i.e., the number of emission sources and/or chemical processes driving the ambient concentrations of the measured species. It therefore allows for the decomposition of the matrix **X** into a product of two matrices: the species profile (f) of each source with dimensions $p \times j$ (representing the repartition of each measured chemical species in the factors) and the contribution (g) of each factor to each sample with dimensions $i \times p$ (representing the time evolution of each factor), allowing for the minimization of the residual error e. This is summarized in Eq. (3):

$$X_{ij} = \sum_{k=1}^{p} g_{ik} \times f_{kj} + e_{ij}. \quad (3)$$

The minimization of the residual sum of squares Q is performed using Eq. (4) to derive the solution for Eq. (3):

$$Q = \sum_{i=1}^{n}\sum_{j=1}^{m}\frac{e_{ij}^2}{\mathbf{S}_{ij}^2} = \sum_{i=1}^{n}\sum_{j=1}^{m}\left[\frac{\mathbf{X}_{ij} - \sum_{k=1}^{p} g_{ik} \times f_{kj}}{\mathbf{S}_{ij}}\right]^2, \quad (4)$$

where $\mathbf{S}_{ij}$ is the uncertainty matrix associated with the data matrix $\mathbf{X}_{ij}$, estimated as described in Sect. 2.2.

The PMF analysis was conducted on a dataset of 42 species, including NMHCs and OVOCs measured by the two online GCs and the PTR-TOF-MS (see Sect. S5), and 329 observations with a time of 1 h 30 min (time resolution of the GCs). Measurements taken by active sampling on sorbent and DNPH cartridges were not included in this dataset due to their low time resolution (3 h), which would have resulted in too few observations. Furthermore, compounds were not considered when missing, when more than half of the observations were below the detection limit or when associated with a low signal-to-noise ratio (< 1 in our case). Missing values and values below the detection limit in the selected dataset were replaced by the geometric mean and half of the detection limit, respectively, following the method used by Sauvage et al. (2009). To minimize the weight of these observations in the PMF results, the uncertainties in the missing values and values below the detection limit were set to 4 times the geometric mean and 5/6 of the detection limit, respectively. PMF also allows for the minimization of the species contributions with low signal-to-noise ratios (< 1.5 in our case) by declaring these species as "weak" and hence tripling their original uncertainties. Fourteen species have been declared as "weak" in this work.

Ethane, methanol and acetone are characterized by high background concentrations at the measurement site. To minimize the weight of these three species in the PMF results, their estimated background concentrations (500, 1000 and 1200 ppt for ethane, methanol and acetone, respectively) were subtracted from the measured concentrations in the data matrix $\mathbf{X}$. These values were chosen arbitrarily to subtract the background concentrations of these species, thereby keeping their variability and avoiding near-zero values.

The PMF was run following the protocol proposed by Sauvage et al. (2009) and relying on several statistical indicators (unexplained part for each factor, correlation between the sum of the factor contributions and the sum of the measured concentration, the parameter Q (see above) and the mean and standard deviation of scaled residuals) to determine the optimal model parameters (number of factors, rotational parameter F_{peak}) leading to the best solution. Based on this approach, we have derived a final solution with six factors for an F_{peak} of -0.5.

Moreover, the homogeneity of the database built using measurements from different techniques was studied to ensure that all instruments are well represented in the solutions. This was done by ensuring that no substantial differences are observed between the scaled residuals of the different instruments. We therefore calculated the mean of the absolute values of the scaled residuals for the three instruments $\left(\overline{\frac{|e_{ij}|}{s_{ij}}}\right)$ (0.73, 0.67 and 0.75 for the PTR-TOF-MS, GC-FID-FID and GC-FID-MS, respectively). The differences observed between these parameters calculated for the three instruments are lower than 0.08. This indicates reasonable homogeneity among the instrument databases (concentrations, uncertainties) since absolute differences below 0.25 have been determined to be satisfactory to avoid overweighting the measurements of a particular instrument in PMF solutions (Crippa et al., 2013a). Therefore, no scaling procedure was performed on the database used in our PMF analysis.

Furthermore, 100 bootstrap runs were performed for the six-factor solution to estimate the stability and uncertainty of this solution. This operation consisted of performing additional PMF runs using new input data files built by randomly selecting nonoverlapping blocks of the original data matrix; the contribution of each factor was derived from these runs and then compared to the original solution. The lowest correlation coefficient between bootstrap solutions and base run solutions was 0.6. The six-factor solution appeared to be well mapped in the base run with a mapping of bootstrap factors to base run factors higher than 86 % for all factors (see Sect. S6).

3.2 Multilinear engine (ME-2)

The source apportionment of organic aerosol components from Q-ACSM was performed using positive matrix factorization (PMF; Paatero, 1997; Paatero and Tapper, 1994) via the ME-2 solver (Paatero, 1999). An extended Q-ACSM dataset of 2 months (from 5 June to 5 August 2013) was used here in order to obtain a wider range of atmospheric variability and improve the PMF output results. The extraction of OA data and error matrices as mass concentrations in $\mu g\,m^{-3}$ over time and their preparation for PMF and ME-2 according to Ulbrich et al. (2009) was done within the ACSM software; the down-weighting procedure of mass fragments, however, was performed using the interface source finder (SoFi; Canonaco et al., 2013) version 6.1. Only m/z up to 100 were considered here since they represented nearly the whole OA mass (around 98 %) and did not interfere with ion fragments originating from naphthalene. The interface SoFI was used to control ME-2 for the PMF runs of the ACSM OA data. Unconstrained PMF runs were investigated here with one to six factors and a moderate number of seeds (10) for each factor number with no conclusive results on the consistency of the mass spectra profiles obtained for the different factors. Constrained PMF runs have been investigated for that purpose with fixed factors for HOA (hydrogen-like OA) with more conclusive results and significant improvements compared to the unconstrained PMF. The results presented

here were obtained for constrained PMF using an averaged HOA profile taken from Ng et al. (2010b) and constrained with a value of 0.1. The properly constrained PMF solution was selected based on the recommendations from Canonaco et al. (2013). These include consistency of the factor profile mass spectra, consistency of times series with external tracers and a low Q/Q_{exp} value. The criteria are presented and discussed hereafter.

In this study, we therefore applied separate factorization analysis to both VOCs and aerosol databases. Another approach consists of a factorization analysis of combined aerosol and gaseous databases (Slowik et al., 2010; Crippa et al., 2013a). Thus, an attempt to perform such PMF analysis was conducted using the gaseous database (42 VOCs) described above and full ACSM spectra as inputs; the homogeneity of the different inputs was taken into account by applying a scaling procedure as proposed by Slowik et al. (2010) and Crippa et al. (2013a). However, it did not allow for the satisfactory apportionment of aerosol measurements and led to weaker solutions than the ME-2 analysis. It was therefore decided to keep separate solutions for gas- and aerosol-phase organics.

3.3 The concentration field model (CF)

Receptor-oriented models have been developed to identify, localize and quantify potential source areas that impact the concentrations of a variable measured at a receptor site in the form of a contribution quantity map. In this study we have used the concentration field (CF) approach developed by Seibert et al. (1994). This method consists of redistributing concentrations of a variable observed at a receptor site along the back trajectories, ending at this site inside a predefined grid ($0.5° \times 0.5°$ for this study). The calculated concentrations in each grid cell are weighted by the residence time that air parcels spent in each cell following Eq. (5):

$$\log \overline{C}_{ij} = \frac{\sum_{L=1}^{M} \left(n_{ijL} \times \log C_L\right)}{\sum_{L=1}^{M} n_{ijL}}, \quad (5)$$

where C_{ij} is the calculated concentration of the ij th grid cell, L is the back-trajectory index, M is the total number of back trajectories, C_L is the concentration measured at the site when the back trajectory L reached it and n_{ijL} is the number of points of the back trajectory L that fall in the ijth grid cell. The latter is representative of the time spent by the back trajectories in the ijth grid cell since a constant time step of 1 h is used between each point of a back trajectory.

The 3-day back trajectories (selected to account for distant potential source areas of species with long lifetimes) used in the CF analysis were calculated by the British Atmospheric Data Centre (BADC) model every hour. This model uses the wind fields calculated by the European Centre for Medium-Range Weather Forecasts (ECMWF) to determine the trajectories of air masses. This model was selected here instead of HYSPLIT for convenience, since the format of the output files matches that needed for our CF model. Comparisons of randomly selected back trajectories in each identified cluster (see Sect. 2.5) calculated by both models (BADC and HYSPLIT) have revealed satisfactory agreement in terms of origin and areas overflown. The BADC back trajectories were interrupted when the altitude of the air mass exceeded 1500 m a.s.l. to get rid of the important dilution affecting air masses in the free troposphere (the boundary layer height has been arbitrarily set here to 1500 m a.s.l. for all trajectories). Furthermore, the grid cells containing fewer than five trajectory points were not considered for robustness purposes.

To take into account the uncertainties associated with the back trajectories, a smoothing of concentrations was applied to all the grid cell values as recommended by Charron et al. (2000) and using Eq. (6):

$$C_{ij-l} = \frac{\left(\sum_{p=1}^{8} C_p + C_{ij}\right)}{9}, \quad (6)$$

where C_{ij-l} is the calculated concentration of the ijth grid cell after smoothing, C_{ij} is the calculated concentration of the grid cell before smoothing and C_p $(1 < p < 8)$ is the concentration before smoothing of the eight neighbor grid cells.

4 Results and discussion

4.1 Overview of gaseous and aerosol measurement results

4.1.1 Gas phase

The measured mixing ratios of some organics (acetylene, isoprene, sum of monoterpenes and acetone), inorganic trace gases (CO, NO, NO_2 and O_3) and wind direction are presented in Fig. 4. Anthropogenic long-lived species, such as acetylene and CO, present similar temporal variations during the campaign. We noticed a slow variation in these compounds with a rise at the beginning of the campaign that reaches a maximum on 21 July with a subsequent decrease. The maximum corresponds to a period when air masses came from areas with strong emissions of anthropogenic species (north of Italy). However, the rise observed on the previous days did not correspond to a specific air mass cluster. The levels of anthropogenic species are very low at the measurement site (below 200 ppt for acetylene, also observed for other anthropogenic compounds; e.g., below 80,

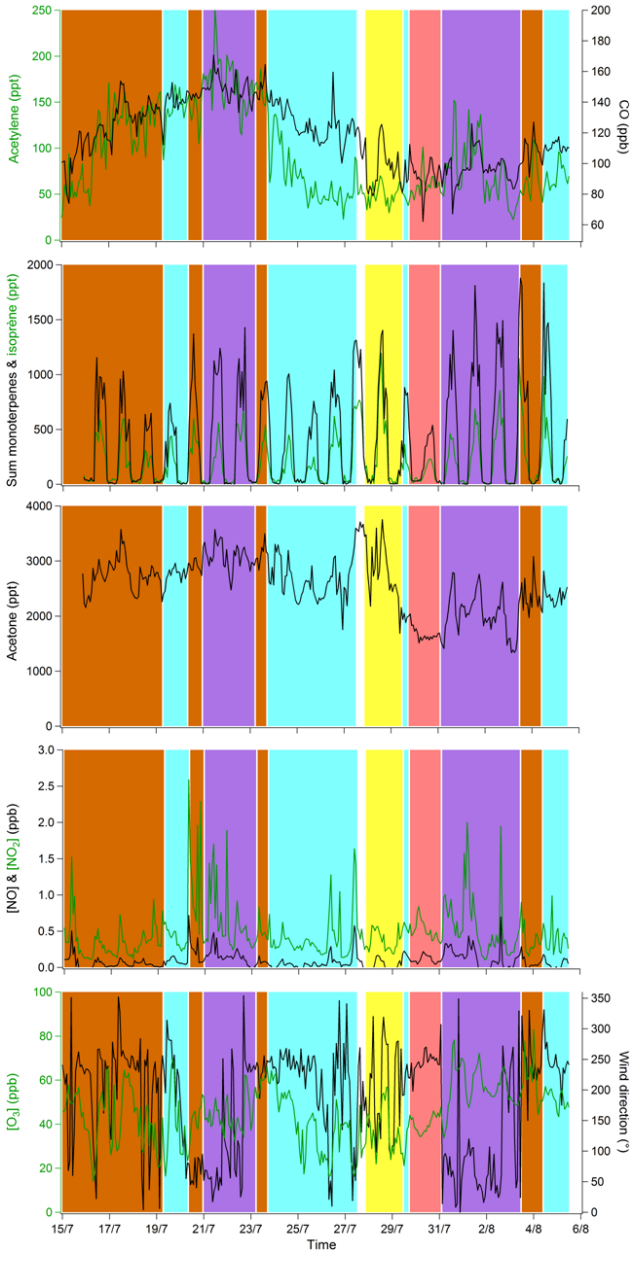

Figure 4. Time series of selected trace gases and wind direction at Cape Corse during the ChArMEx SOP2 field campaign. The colored areas correspond to back-trajectory clusters (light blue, purple, yellow, pink and orange-brown for the marine west, Europe northeast, Corsica south, France northwest and calm low wind clusters, respectively).

120 and 150 ppt for benzene, *n*-butane and toluene, respectively) highlighting the probable lack of local anthropogenic sources. These very low levels of anthropogenic species at the ground level (often close to the limit of detection) made their measurements very challenging during the campaign.

In contrast, significant levels of primary biogenic compounds were observed and could reach up to 1.2 and 2.0 ppb for isoprene and the sum of monoterpenes, respectively (Fig. 4). These compounds were locally emitted by the typical vegetation in the Mediterranean region ("maquis" shrubland) surrounding the measurement site. The mixing ratios for these compounds present a clear diurnal cycle with the highest values coinciding with maxima of temperature and solar radiation. Two periods characterized by high mixing ratios of biogenic VOCs were observed (27–28 July and 2–4 August), which correspond to the warmest periods of the campaign.

Oxygenated VOCs, such as acetone, were also present at significant levels of up to 3.8 ppb (Fig. 4). This compound has primary and secondary sources from the oxidation of both biogenic and anthropogenic VOCs (see discussion in Sect. 4.2.3). Therefore, acetone levels increase both when anthropogenic VOC concentrations increase (first part of the campaign) and when intense biogenic emissions are observed (27–28 July and 2–4 August).

NO_x levels remained low (< 0.5 and < 2.0 ppb for NO and NO_2, respectively) during the whole campaign. This confirms the lack of local anthropogenic sources close to the measurement site. Levels of O_3 were very variable (20–80 ppb) with the highest levels encountered during the last part of the campaign. This period corresponded to the warmest period with intense biogenic emissions, but also to air masses originating from the north of Italy, an area characterized by intense anthropogenic emissions of ozone precursors.

Oxygenated VOCs (including primary and secondary OVOCs from anthropogenic and biogenic origins) largely dominate the speciation of the measured VOCs (78–80 %; see Fig. S7). OVOCs are dominated by methanol, acetone and formic acid, which represent 28, 23 and 14 % of total OVOCs, respectively. The weak contribution of biogenic hydrocarbons to the total VOC composition (4–5 %; see Fig. S7) is due to the fact that these contributions are calculated on a 24 h basis and not only during daytime when their concentrations are more elevated.

Finally, anthropogenic NMHCs represent only 15–18 % of the measured VOCs (see Fig. S7), which is consistent with the remote location of the site. This VOC family is dominated by ethane, propane and ethylene, which represent 34, 7 and 7 % of total A-NMHCs, respectively. However, it is worth noting that this apportionment is only valuable for the measured species. The difference between the measured OH reactivity (total sink of OH) and the calculated one using all measured compounds reported for this campaign indicates that approximately 56 ± 15 % (1σ on average) of the measured OH reactivity was missing. The largest fraction of missing OH reactivity was observed between 23 and 30 July, a period associated with the marine west and south clusters (Zannoni et al., 2016). Therefore, a large fraction of the

VOCs composing the air masses reaching the site has not been measured yet.

4.1.2 Aerosol phase

The chemical composition derived from the Q-ACSM measurements is reported in Fig. 5a for the period of study (15 July to 5 August) and shows a clear and permanent dominance of OM, which represents 55 % of the total mass of NR-PM_1 on average (average of 3.74 ± 1.80 $\mu g\,m^{-3}$), followed by sulfate (27 %, 1.83 ± 1.06 $\mu g\,m^{-3}$), ammonium (13 %, $0.90 \pm 0.55\,\mu g\,m^{-3}$) and nitrate (5 %, $0.31 \pm 0.18\,\mu g\,m^{-3}$). These values are in the range of the monthly mean concentrations for summer calculated with Q-ACSM data over the 2-year measurement period (June 2012 to July 2014) performed at the measurement site (J. Sciare, unpublished data). OM concentrations are comparable to those observed by Sciare et al. (2008) in the eastern Mediterranean for the month of July ($[OC] = 2.18 \pm 0.65\,\mu g\,m^{-3}$ using an OM-to-OC ratio of 1.9; Sciare et al., 2003). OA concentrations in Ersa are also comparable to those observed between June 2012 and July 2013 by Minguillón et al. (2015) at a site in northern Spain 25 km from the Mediterranean coast ($OA = 3.8\,\mu g\,m^{-3}$ on average) and to those measured by Debevec et al. (2017) in the eastern basin in Cyprus ($OA = 3.33\,\mu g\,m^{-3}$ on average). Comparable concentrations for ammonium and sulfate were also found by Minguillón et al. (2005; on average 0.8 and 1.3 $\mu g\,m^{-3}$, respectively), while they observed higher nitrate concentrations (0.8 $\mu g\,m^{-3}$ on average). It is worth noting that Minguilloón et al. (2005) report yearly measurements and not only summer measurements as in this study.

The overall OA concentrations during the campaign vary within 2 orders of magnitude (ranging from 0.13 to 9.77 $\mu g\,m^{-3}$) with very short periods (1 to 4 h) characterized by very sharp drops (close to zero) associated with clouds passing the station and the subsequent uptake of fine aerosols into the cloud droplets.

The temporal variability in OC and WSOC is reported in Fig. 5b and shows very close patterns with a few periods of noticeable discrepancies (17 and 28–30 July). There is a clear correlation between the two datasets ($r^2 = 0.68$; $N = 229$); the slope of 0.58 reflects the fact that more than half of OC is water soluble. The correlation between OC (OCEC Sunset field instrument) and OM (Q-ACSM) shows better agreement ($r^2 = 0.86$; $N = 229$) with a slope of 0.87 when using an OC-to-OM ratio of 1.9. This slope of close to 1 reflects the generally good agreement between the instruments measuring OC in $PM_{2.5}$ and OM in PM_1, respectively. A closer look at the OM / OC ratio derived from these two instruments (not shown) shows a slight but systematic diurnal variability with minimum values at around 09:00 LT and a constant rise in the course of the day with a maximum value at 21:00 LT. Interestingly, although the absolute OM / OC ratio calculated empirically from Q-ACSM mass spectra (Aiken et al., 2008)

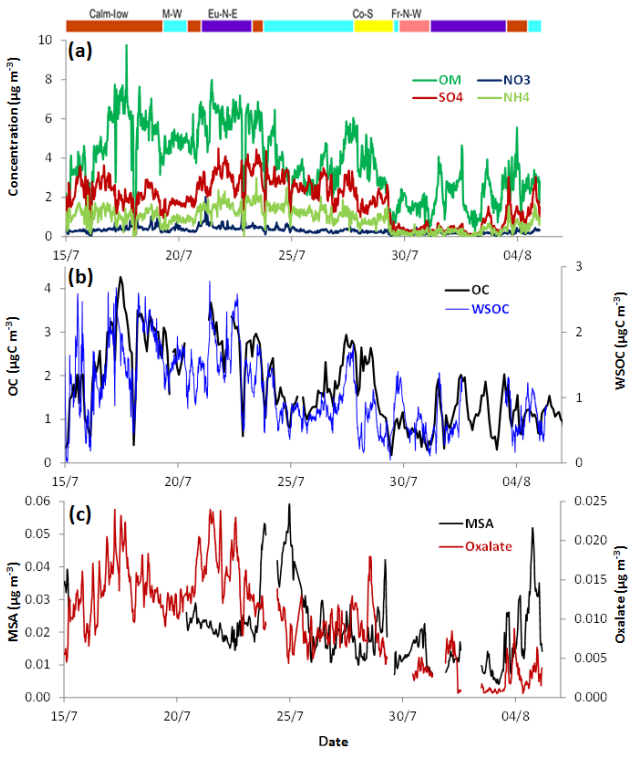

Figure 5. Temporal variability at Cape Corse in **(a)** submicron (NR-PM_1) chemical constituents measured by ACSM. **(b)** OC ($PM_{2.5}$) and WSOC (PM_1) measured by OCEC Sunset field instrument and PILS-TOC. **(c)** MSA and oxalate (PM_{10}) measured by PILS-IC. The colored areas at the top correspond to back-trajectory clusters: light blue, purple, yellow, pink and orange-brown for the marine west (M-W), Europe northeast (Eu-N-E), Corsica south (Co-S), France northwest (Fr-N-W) and calm low wind (calm-low) clusters, respectively.

should be interpreted with caution (Crenn et al., 2015), its temporal variability shows exactly the same diurnal pattern of local photochemical oxidation of OA. This provides further consistency for our Q-ACSM fragmentation data, which will be used later in the source apportionment.

Real-time observations of two light organic tracers (MSA and oxalate) are reported in Fig. 5c. MSA (methanesulfonic acid, CH_3SO_3H) is an oxidation end product of dimethyl sulfide (DMS), a natural gas produced from marine phytoplankton activity. MSA is mostly in the aerosol phase and formed through the heterogeneous oxidation of dimethyl sulfoxide (DMSO). It has been recently used to infer a marine organic aerosol (MOA) source from a source apportionment study performed in the region of Paris (France; Crippa et al., 2013b). Oxalic acid is the most abundant dicarboxylic acid in the troposphere (Kawamura et al., 1996). Its primary sources cannot solely explain its observed ambient concentrations (Huang and Yu, 2007), suggesting that secondary formation processes remain significant (Warneck, 2003). Simulations of these compounds predict reactions through in-cloud pro-

cessing (Carlton et al., 2007; Ervens et al., 2004, 2008; Fu et al., 2008; Lim et al., 2005; Myriokefalitakis et al., 2011; Sorooshian et al., 2006; Volkamer et al., 2007; Warneck, 2003). Field measurements also provided evidence of heterogeneous chemistry in the formation of oxalic acid through different routes (Crahan et al., 2004; Sorooshian et al., 2006, 2007). Consequently, real-time observations of MSA and oxalate may be used here in our source apportionment study to infer secondary oxidation processes.

4.2 Exploring the drivers of VOC variability at Cape Corse

Source-receptor models, such as PMF, usually aim at identifying and quantifying the contributions of sources of pollutants impacting a measurement site. In our case, the remote location of the site combined with the reactivity of the selected species does not allow for the proper identification and quantification of primary sources. Our main objective here is the identification of covariation factors of species that could be representative of aged or fresh primary emission and also of photochemical processes occurring during long-range transport or occurring locally. For this purpose, PMF was applied to a large dataset (42 different species), including primary VOCs from anthropogenic or biogenic origins, and also secondary products measured by three different techniques (PTR-TOF-MS, GC-FID-FID and GC-FID-MS; see Sect. 2.2).

Figure 6 shows the time series of the six factors obtained by the PMF analysis. Figure 7 shows the contributions of each factor to the species selected as inputs for the PMF model (in %) and the absolute averaged contribution of each species to the six factors determined by the PMF analysis (in ppt). Finally, Fig. 8 presents the maps of simulated contributions (in ppt) using the CF model for four of the six PMF factors. The relative contributions of the different PMF factors to the sum of species used as inputs are presented in Fig. S8.

4.2.1 Anthropogenic influence

Among the six PMF factors, three different factors were attributed to primary anthropogenic sources (factors 2, 3 and 5) and are characterized by compounds with various lifetimes (Figs. 6 and 7). The lifetimes reported below are estimated from kinetic rate constants of the reactions between the species of interest and OH, assuming an averaged OH concentration of 2.0×10^6 molecules cm^{-3}.

Factor 2 is composed of long-lived primary anthropogenic species, such as ethane (58 % explained by factor 2), acetylene (44 % explained), propane (30 % explained) and benzene (45 % explained; see Fig. 7), with lifetimes ranging from 5 to 25 days and typically emitted by natural gas use and combustion processes. In addition to these long-lived primary anthropogenic species, other anthropogenic NMHCs with shorter lifetimes compose this factor, such as ethylene (35 % explained) or 2-methyl-2-butene co-eluted with 1-pentene (42 % explained). It tends to indicate that in addition to the lifetime, the nature of the sources (e.g., combustion processes) also partly influences the profile of this factor. Furthermore, factor 2 exhibits behavior similar to CO (see Sect. S9), a long-lived compound (lifetime of $\sim$ 24 days) mainly emitted by combustion processes, which supports the identification of this factor as long-lived anthropogenic. Hence, the lack of diurnal variability in this factor (see Sect. S10) confirmed its long-range origin. The potential source areas associated with this factor (Fig. 8) are the north of Italy (Po Valley), the southeast of France and, to a lesser extent, the northeast of Tunisia (area of Tunis). These areas, particularly the Po Valley, are known to supply high anthropogenic emissions due to intense industrial activities and a dense road network (Thunis et al., 2009). This result strengthens the assumption of a primary anthropogenic origin for this factor. This factor represents 16–17 % of the sum of VOC species used as inputs in the PMF model (Fig. S8).

Factor 3 is composed of medium-lived primary anthropogenic species, such as *n*-pentane (78 % explained by factor 3), isopentane (68 % explained) and 2,2-dimethylbutane (48 % explained; see Fig. 7) with lifetimes ranging from 1 to 3 days and typically emitted by gasoline evaporation or vehicle exhaust. This factor shows higher levels for air masses coming from the Europe northeast and the France northwest sectors (see Fig. 6). Consequently, the north of Italy (Po Valley) and the southeast of France, which are areas experiencing high anthropogenic emissions, are also identified as potential source areas for this factor (Fig. 8). Potential source areas identified in the center of France are most likely falsely attributed to this area due to the corridor effect: the air masses reaching Cape Corse and passing over the center of France systematically encompass source areas (southeast of France). This factor represents 12 % of the sum of VOC species used as inputs in PMF model (Fig. S8).

Factor 5 is composed of short-lived primary anthropogenic VOCs, such as ethylene (38 % explained by factor 5), propene (44 % explained) and toluene (38 % explained), with lifetimes ranging from 5 to 23 h and typically emitted by combustion processes. This factor exhibits higher levels for air masses coming from the Corsica south sector (see Fig. 6). Likewise, areas in the south of Corsica are identified as potential source areas for this factor (Fig. 8). Emissions from these areas could be due to intense ship emissions, for which speciation is dominated by alkenes (ethene, propene), aromatics and heavy alkanes ($> C_6$; Eyring et al., 2005). A contribution from the Corsican cities in this southern sector cannot be excluded. This factor represents 21–23 % of the sum of species used as inputs in the PMF model (Fig. S8).

The total contribution of anthropogenic-like factors to the sum of species used as inputs in the PMF model is in the range of 49–52 %. This is higher than the contributions of anthropogenic NMHCs relative to measured VOCs (15 %, see Fig. S7). This can be explained by the fact that anthro-

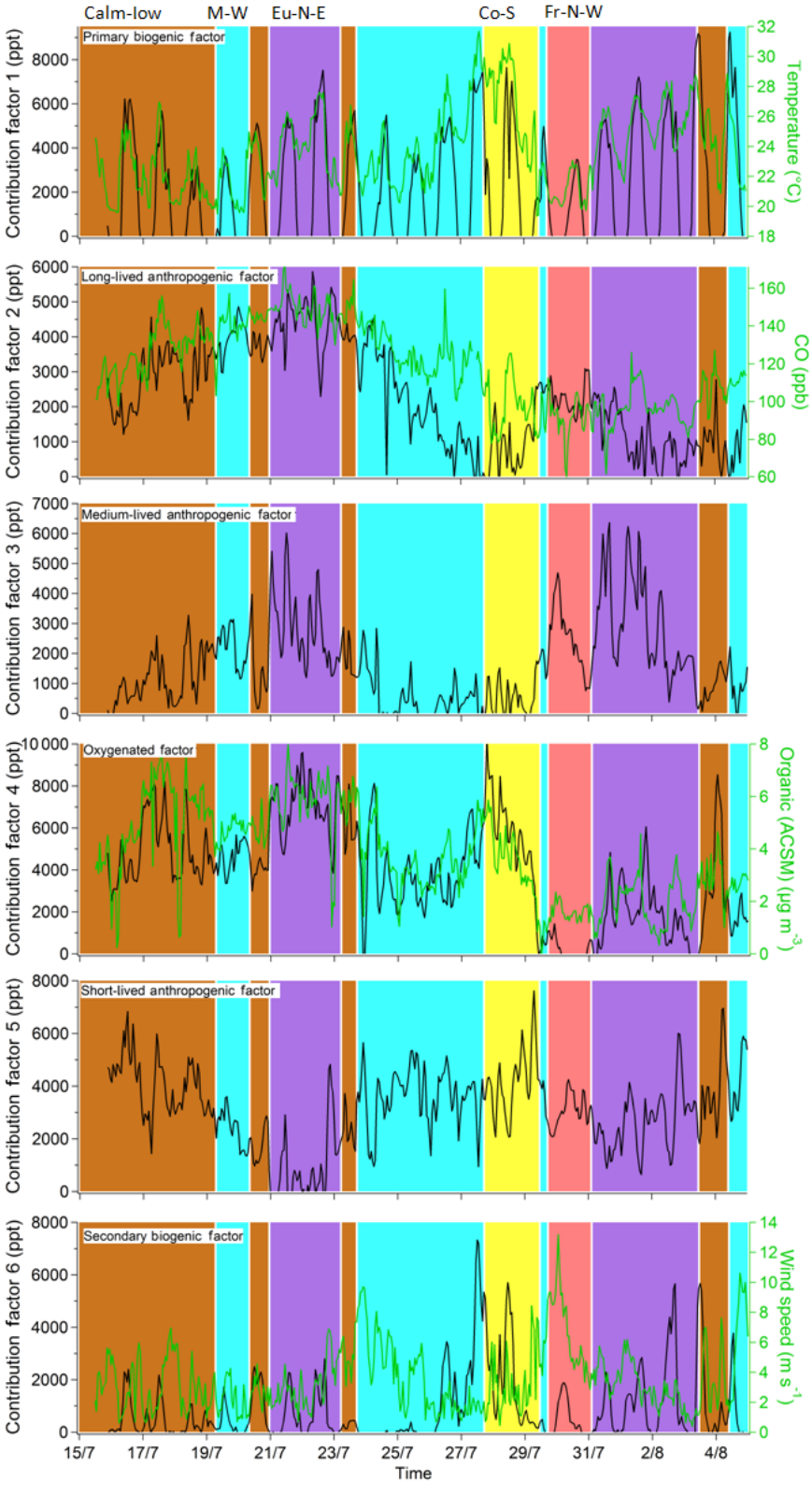

Figure 6. Time series for the contribution of the six gas-phase PMF factors together with temperature, CO, the measured organic fraction of aerosols and wind speed. The colored areas correspond to back-trajectory clusters: light blue, purple, yellow, pink and orange-brown for the marine west (M-W), Europe northeast (Eu-N-E), Corsica south (Co-S), France northwest (Fr-N-W) and calm low wind (calm-low) clusters, respectively.

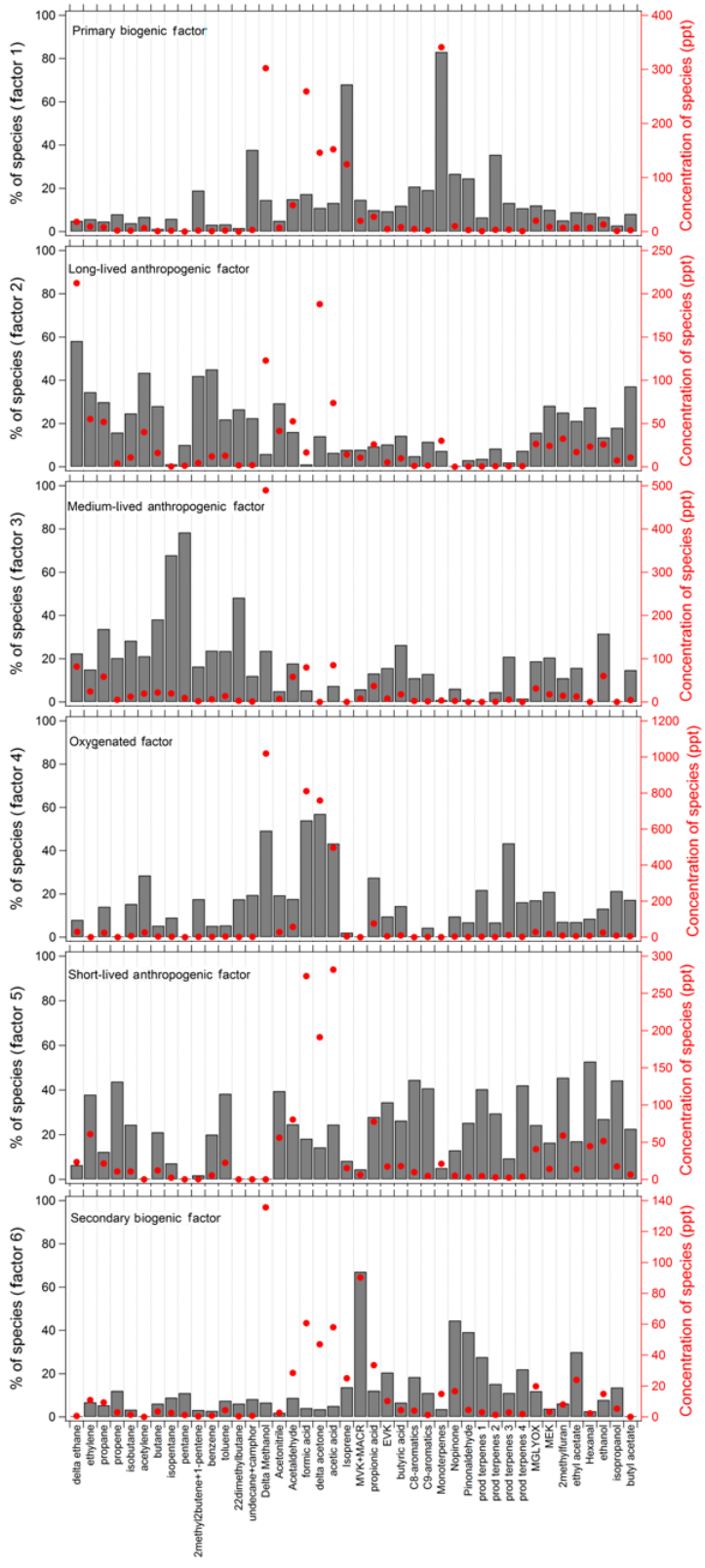

Figure 7. Profiles of the six gas-phase PMF factors with contributions of the factors to each species (black histograms; left axis in %) and contributions of the species to each factor (red circles; right axis in ppt). The "prod terpenes" 1, 2, 3 and 4 correspond to the m/z 99, 111, 113 and 155 signals from the PTR-TOF-MS measurements, respectively, which have been attributed to oxidation products of terpenes (Holzinger et al., 2005; Lee et al., 2006; Vlasenko et al., 2009; Fares et al., 2012; Park et al., 2013).

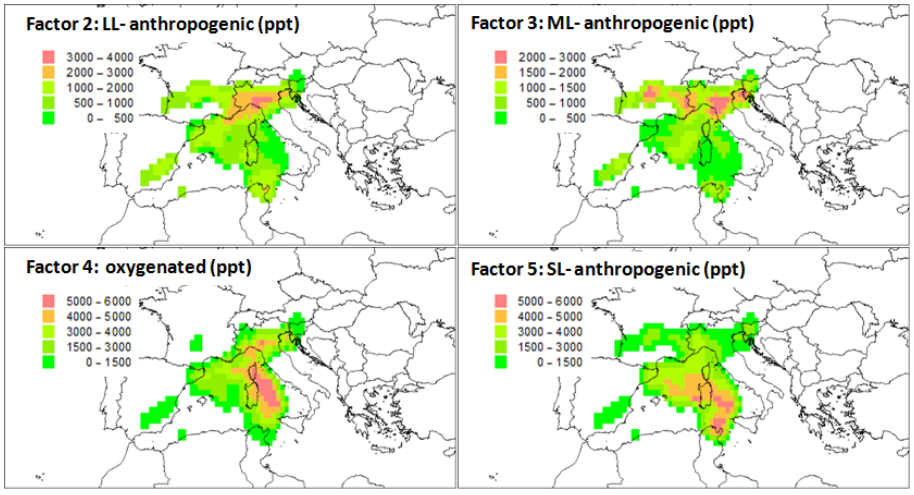

Figure 8. Source identification for the six gas-phase PMF factors using the CF model. Contributions are in parts per trillion (ppt).

pogenic NMHCs not only contribute to these anthropogenic factors, but some OVOCs are also part of them. For example, methanol and acetone both contribute to a non-negligible extent to these anthropogenic factors. Methanol contributes to 7 and 39 % of LL anthropogenic factors and ML anthropogenic factors, respectively; acetone contributes to 14 and 11 % of LL anthropogenic factors and SL anthropogenic factors, respectively. Therefore, higher contributions of these factors to the gas-phase composition are expected. Considering the primary anthropogenic part of OVOCs determined based on the anthropogenic factor contribution to OVOCs, the contribution of anthropogenic VOCs to measured VOCs rises to 42 % (see Fig. 9), which is much closer to the PMF results.

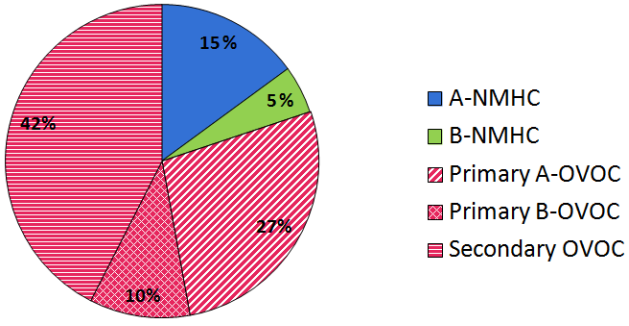

Figure 9. Distribution of the different VOC groups (ANMHC is anthropogenic NMHCs, blue; BNMHC is biogenic NMHCs, green; OVOC is oxygenated VOCs, pink) calculated from the database used for PMF analysis (same as bottom panel of Fig. S7). The OVOC group is divided into three subclasses to account for their different origins: primary anthropogenic (primary A-OVOC, diagonal stripes), primary biogenic (primary B-OVOC, grid pattern) and secondary origin from the oxidation of both anthropogenic and biogenic VOCs (secondary OVOC, horizontal stripes). The partitioning of these OVOCs into the three subclasses is described in Sect. 4.2.4.

4.2.2 Biogenic influence

Among the six factors, two biogenic factors are also clearly identified (factors 1 and 6). They are respectively composed of primary biogenic species (factor 1) and oxidation products of primary biogenic hydrocarbons (factor 6). Therefore, they have been classified and will be respectively reported in the following as the "primary biogenic factor" (factor 1) and "secondary biogenic factor" (factor 6).

Factor 1 is composed of primary biogenic species with very short lifetimes emitted locally by the vegetation surrounding the measurement site, such as isoprene (68 % explained by factor 1), the sum of monoterpenes (83 % explained) and camphor co-eluted with undecane (38 % explained; see Fig. 7). This factor exhibits clear diurnal cycles (Figs. 6 and S9) and is correlated, as expected, with temperature (see Sect. S9), which is known to influence biogenic emissions together with solar radiation (Guenther et al., 1995, 2000).

This factor represents 14 % of the sum of species used as inputs in the PMF model (Fig. S8). This is higher than the contributions of biogenic NMHCs to measured VOCs (4–5 %; see Fig. S7). As already proposed for anthropogenic factors, this can be explained by the fact that biogenic NMHCs not only contribute to these primary biogenic factors, but some biogenic OVOCs can also be part of them. For example, carboxylic acids, methanol and acetone also contribute 13, 15 and 11 % on average, respectively (explained by factor 1). Taking into account the primary biogenic part of OVOCs, the contribution of biogenic VOCs to measured VOCs rises to 15 % (see Fig. 9), which is closer to the PMF results.

Factor 6 is composed of oxidation products of primary biogenic VOCs, such as methyl vinyl ketone (MVK) and methacrolein (MACR; 67 % explained by factor 6), which

are measured as a sum by PTR-TOF-MS (m/z 71.05), nopinone (45 % explained) and pinonaldehyde (39 % explained; see Fig. 7). More specifically, MVK and MACR are first-generation oxidation products of isoprene (Miyoshi et al., 1994), nopinone is a first-generation oxidation product of β-pinene (Wisthaler et al., 2001) and pinonaldehyde is a first-generation oxidation product of α-pinene (Wisthaler et al., 2001). As expected, the variability in this factor is also correlated with temperature (see Sect. S9). It can be explained by higher emissions of primary biogenic VOCs under warmer conditions associated with more intense photochemistry. Furthermore, the lowest levels of factor 6 correspond to the highest wind speed observed at the measurement site and vice versa (see Fig. 6); near-zero contributions of factor 6 are observed on 23–25 July when wind speeds were between 3 and 10 m s^{-1}. In contrast, the highest diurnal maxima were observed on 26–28 July and on 2 and 3 August when wind speeds did not exceed 3 m s^{-1}. This factor is characterized by first-generation oxidation products of primary biogenic VOCs emitted in the vicinity of the site, and low wind speeds are necessary to observe them at significant levels. In the case of high wind speeds, these oxidation products undergo fast transport and dilution, and low levels might be observed. This factor represents 6 % of the sum of species used as inputs in the PMF model (Fig. S8) and is therefore the less important.

4.2.3 Oxygenated factor

The last factor (factor 4) has been interpreted as an "oxygenated factor" since it is mainly characterized by OVOCs, such as carboxylic acids (54 % formic acid, 43 % acetic acid, 28 % propionic acid and 14 % butyric acid), alcohols (49 % methanol and 21 % isopropyl alcohol) and carbonyls (57 % acetone, 18 % acetaldehyde and 21 % methyl ethyl ketone). Most of these species are formed by the oxidation of both anthropogenic and biogenic compounds, although some of them can also be directly emitted into the atmosphere and can therefore be of both primary and secondary origin. For example, methanol (the highest contributor to factor 4) can be emitted by vegetation (MacDonald and Fall, 1993), biomass burning (Holzinger et al., 1999) or urban and industrial activities (Hu et al., 2011). It can also be formed by photochemistry (mainly the photooxidation of methane; Tyndall et al., 2001). The same is true for acetone (the second-highest contributor to factor 4). Acetone can be directly emitted from vegetation (Goldstein and Schade, 2000; Hu et al., 2013), biomass burning (Simpson et al., 2011) and anthropogenic sources (Hu et al., 2013), and it can also be formed via the photochemical oxidation of anthropogenic VOCs, such as alkanes (Goldstein and Schade, 2000), and biogenic VOCs, such as monoterpenes (Reissell et al., 1999). Note that the same is true for carboxylic acids, which also have multiple sources (de Angelis et al., 2012 and references therein).

The multisource pattern for this factor is highlighted by its time series. Factor 4 exhibits similar behavior as anthropogenic factors (factors 2 and 3) at the beginning of the campaign with an increase to reach a maximum around 21 July and then a decrease. This factor rises again during the intense biogenic-influenced warm period (26–28 July) as observed for the secondary biogenic factor (factor 6).

The CF analysis for this factor leads to the identification of northern Italy and a large area in southern Corsica as potential source regions. The north of Italy may contribute to the anthropogenic continental influence of this factor, while the large regions in the south of Corsica may contribute to the biogenic influence since the highest biogenic signature also corresponds to air masses coming from the Corsica south sector. This could be explained by both potential biogenic emissions from the vegetation in Corsica (the site being at the extreme north of the island) and/or warmer and more stagnant conditions arising when air masses come from the Corsica south sector, favoring local biogenic emissions and low dispersion of oxidation products. It could also be due to local anthropogenic emissions from Corsican cities erroneously attributed to more distant regions, as already observed for the CF analysis of factor 5. Finally, one cannot rule out the possibility of a primary or secondary influence of ship emissions to factor 4 for this potential source area. This is also in accordance with the non-negligible contribution of this factor to the acetylene variability (29 % explained by this factor). This factor represents 28–31 % of the sum of species used as inputs in the PMF model (Fig. S8) and is therefore the most important one. Combined with the secondary biogenic factor, it leads to a contribution of 34–37 % for the oxygenated factors. This is significantly lower than the OVOC contribution to the actual measured VOCs (80 %; see Fig. S7) and can be explained by the contribution of most OVOCs, such as acetone, methanol and carboxylic acids, to other PMF factors. When only considering the secondary part of measured OVOCs, their contribution to measured VOCs decreases to 42 % (see Fig. 9), which is closer to the PMF results.

4.2.4 Apportionment of measured OVOC

From the six PMF factors, it is possible to apportion the measured OVOCs among their potentially different origins (primary anthropogenic or biogenic emissions, photochemical production from the oxidation of anthropogenic or biogenic hydrocarbons). Therefore, factor 1 is attributed to a primary biogenic origin, while factors 2, 3 and 5 are attributed to a primary anthropogenic origin, and factors 4 and 6 are attributed to a secondary origin (photochemical oxidation of primary VOCs from both biogenic and anthropogenic origins). The contributions of each OVOC to a specific PMF factor are summed up and ascribed to the corresponding origin. The subtracted backgrounds of acetone and methanol are redistributed to each PMF factor according to the relative contribution of these species to each factor. The appor-

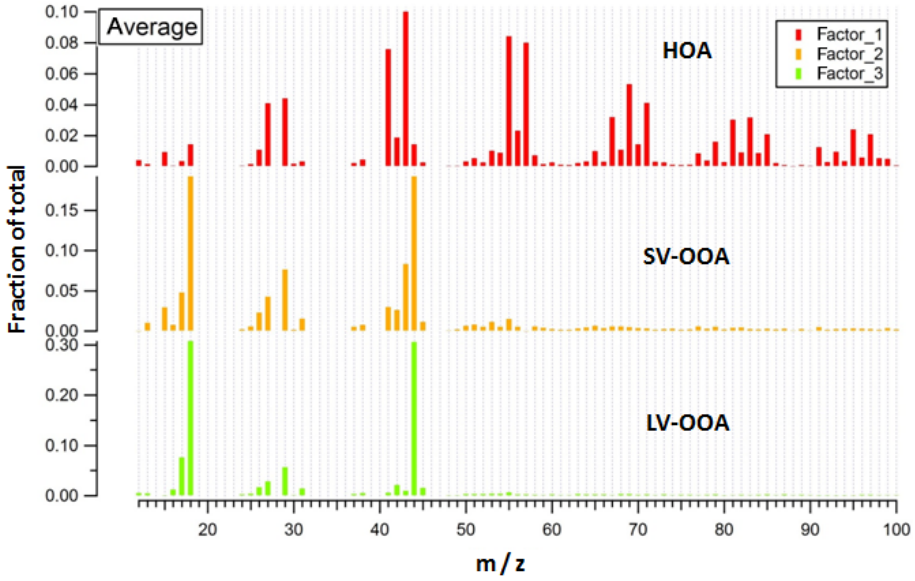

Figure 10. Mass spectra profile obtained for the three-factor-constrained PMF solution (factor 1 = HOA, red; factor 2 = SV-OOA, orange; factor 3 = LV-OOA, green).

tionment of anthropogenic, biogenic and secondary origins for OVOCs can be seen in Fig. 9. Primary anthropogenic sources, primary biogenic sources and secondary processes account for 34, 13 and 53 % of the measured OVOCs, respectively. Therefore, the measured OVOCs at Cape Corse are approximately half oxidation products of VOCs and half primary VOCs.

4.2.5 Comparison with other PMF studies performed in remote environments

To our best knowledge, only three studies have been conducted that applied PMF for gas-phase species in remote environments (Sauvage et al., 2009; Lanz et al., 2009; Leuchner et al., 2015). These studies were only based on NMHC measurements and chlorinated organic species in one case (Lanz et al., 2009). No oxygenated VOCs were considered. Consequently, these three studies only identified factors representative of primary sources.

Leuchner et al. (2015) identified six PMF factors at a remote site at Hohenpeissenberg over a period of 7 years (2003–2009), including primary biogenic, short-lived combustion, short-lived evaporative, residential heating, long-lived evaporative and background factors. The classification of factors was linked to the difference in the source typology (biogenic versus anthropogenic, combustion versus evaporative) and/or the lifetime of compounds (short-lived versus long-lived). Lanz et al. (2009) found only four PMF factors at a continental mountain site at Jungfraujoch (Switzerland) over 8 years (2000–2007), including a highly aged combustive emission factor correlated with CO, a fresh emission and solvent-use factor correlated with NO_x and two industrial factors mainly explaining the variability in chlorinated compounds. Sauvage et al. (2009) applied PMF to a database of NMHCs measured at three background sites in France, leading to five common PMF factors, including evaporative sources, residential heating, vehicle exhaust, remote sources attributed to aged background air and biogenic emissions.

Therefore, we incorporated OVOCs for the first time in a database used for PMF analysis at a remote environment. It allows for the first identification of the PMF factors representative of secondary processes in addition to factors related to primary sources. As has been found in previous studies performed in such environments, we also found that primary anthropogenic PMF factors were separated according to the lifetime of the compounds that composed them. As in the three studies described above, a clear primary biogenic factor is identified in our study. Furthermore, our analysis allowed for the apportionment of the anthropogenic, biogenic and secondary parts of OVOCs.

4.3 Source apportionment of OA at Cape Corse

Based on the two available months of ACSM data, a three-factor solution was selected here, corresponding to a minimum of the quality parameter Q/Q_{exp}. The mass spectra reported in Fig. 10 show a typical HOA (hydrogen-like OA) profile for the first factor with n-alkanes, branched alkanes, cycloalkanes and aromatics, leading to high signals in the ion series $C_nH^+_{2n+1}$ and $C_nH^+_{2n-1}$ (m/z 27, 29, 41, 43, 55, 57, 69, 71) that are typical for fossil fuel combustion (Canagaratna et al., 2004; Chirico et al., 2010). We have also used the terms "SV-OOA" (semi-volatile oxygenated organic aerosol) and

"LV-OOA" (low volatility OOA) as introduced by Jimenez et al. (2009) to describe the two remaining factors. In these two factors, m/z 43 and 44 are the most prominent peaks, which is consistent with OOA (oxygenated OA) spectra and the m/z 44 to 43 ratio that increases with aging (Ng et al., 2010a). The signal at m/z 43 is dominant for the second factor and mainly comes from the fragmentation of either hydrocarbon chains to form $C_3H_7^+$ or carbonyls to form $C_2H_3O^+$; therefore this factor appears to be less oxidized and was consequently named SV-OOA.

The consistency of the different OA factors was further checked with the external tracers in Fig. 11; HOA with BC (fossil fuel tracer), SV-OOA with WSOC and LV-OOA with oxalate. The good agreement of SV-OOA with WSOC is consistent with freshly formed SOA being semi-volatile and water soluble as reported, for instance, by Hennigan et al. (2008a) who observed strong similarities between semi-volatile NH_4NO_3 and (PILS-TOC-based) WSOC. The good agreement between LV-OOA with oxalate is consistent with the fact that both are mostly composed of carboxylic acid COO chains and the use of oxalate as a proxy for highly oxidized OA, as stated before. Also note that good correlation is obtained between the averaged OOA mass spectra taken from Ng et al. (2010b) and our two factors with correlation coefficients (r^2) of 0.96 and 0.81 for our SV-OOA and LV-OOA factors, respectively.

The different OA factors obtained here are mainly of continental origin, and therefore their temporal variability is mostly related to the amount and frequency of continental air masses reaching the sampling site. Nevertheless, the diurnal variation in SV-OOA and LV-OOA (Fig. S11) suggests that local photochemical processes have also occurred, with local formation of fresh SV-OOA in the morning followed by rapid oxidation, which could explain the enhancement of LV-OAA in the afternoon.

Average mass concentrations are 0.13, 1.59 and 1.92 $\mu g\,m^{-3}$ for the three determined factors HOA, SV-OOA and LV-OOA, respectively, for a total average OA concentration of 3.63 $\mu g\,m^{-3}$ and a contribution of OA to NR-PM_1 of 52 %. As a result, secondary OA represents about 96 % of OA with aged (LV-) OOA contributing approximately 55 % of this secondary OA fraction. In recent years, increasing background OA observations have become available in the Mediterranean, mostly at coastal sites located in the northern part of the basin (Spain, France, Italy and Greece). For instance, long-term (13-month) ACSM measurements were performed at a regional background site in the western Mediterranean (Spain) located in Montseny Natural Park 50 km north-northeast of Barcelona, approximately 500 km west of Cape Corse. Reported observations are similar to ours with an OA contribution to NR-PM_1 of ca. 60 % (Minguillón et al., 2015), three major OA sources (HOA, SV-OOA and LV-OOA) during summer with a very prominent secondary fraction (85 % of OA) and OA profiles very similar to those obtained here.

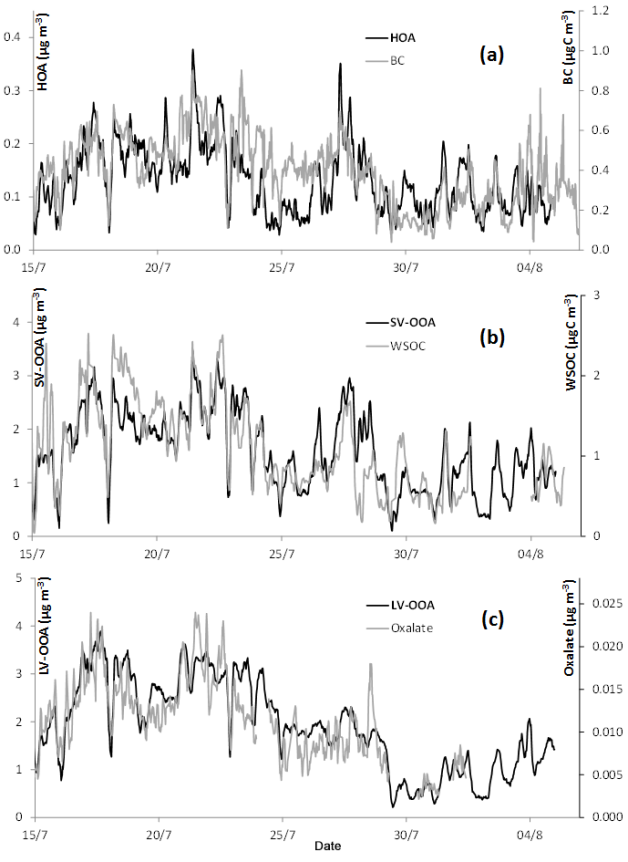

Figure 11. Time-series of **(a)** HOA (black) with black carbon (gray), **(b)** SV-OOA (black) with WSOC (gray) and **(c)** LV-OOA (black) with oxalate (gray).

4.4 Gas–aerosol link

First, the gas-phase "oxygenated factor" (factor 4) is correlated with the organic fraction of the aerosol measured by ACSM ($R^2 = 0.58$, $n = 498$; see Sect. S9). This fair correlation likely highlights the close link between gaseous oxidation products observed at the site and measured organic aerosol (OA) since they stem from similar processes. During the campaign, very low levels of primary organic aerosols were observed (HOA determined by ACSM measurements below 0.4 $\mu g\,m^{-3}$; see Fig. 11a, top panel). Thus, this correlation is most likely due to the secondary fraction of OA, representing 96 % of OA (see Sect. 4.3), which can come from the oxidation of both biogenic and anthropogenic gaseous precursors; this explains the similar behavior of factor 4.

Figure 12 shows stacked time series of the different fractions (inorganic and organic) of aerosol measured by ACSM (top panel) and stacked time series of contributions of PMF factors (middle panel) for the VOCs (see Sect. 4.2). This figure aims to draw a parallel between aerosol- and gas-phase compositions to highlight the link between the two phases.

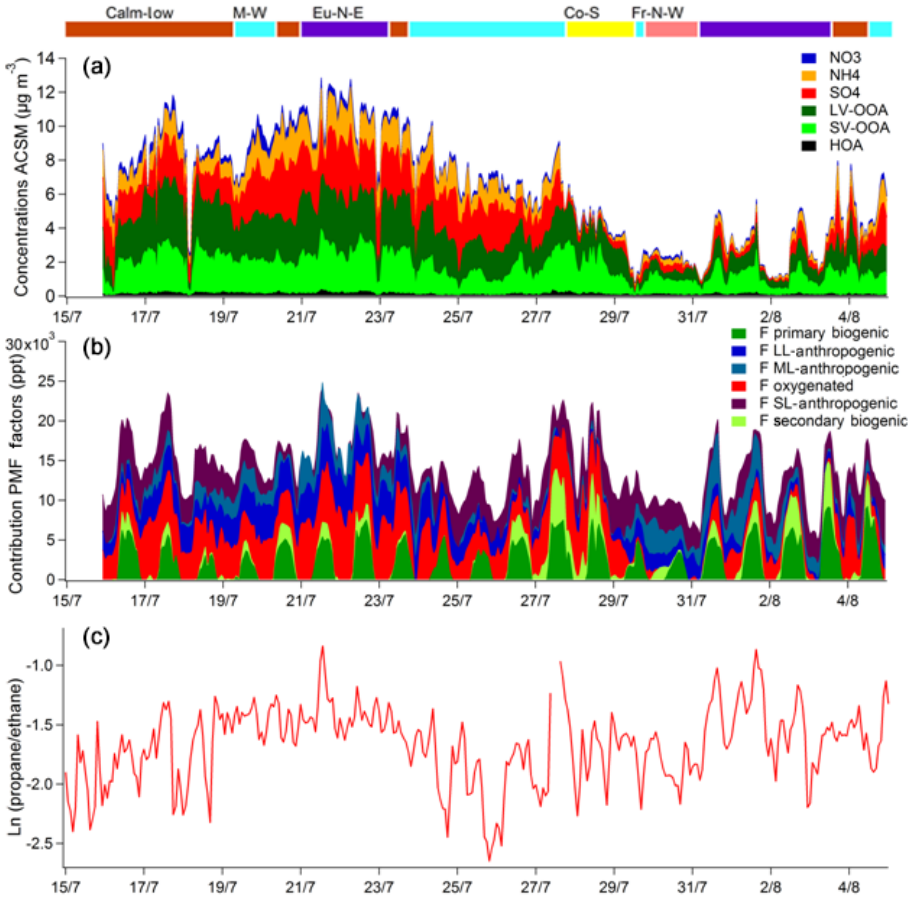

Figure 12. Stacked time series of aerosol fractions (top panel), VOC PMF factors (middle panel) and ln(propane / ethane) as a proxy for photochemical age (bottom panel). F-LL, F-ML and F-SL anthropogenic refer to the long-lived, medium-lived and short-lived anthropogenic factors, respectively. The colored areas at the top correspond to back-trajectory clusters: light blue, purple, yellow, pink and orange-brown for the marine west (M-W), Europe northeast (Eu-N-E), Corsica south (Co-S), France northwest (Fr-N-W) and calm low wind (calm-low) clusters, respectively.

From these graphs and from the back-trajectory clusters (also shown in Fig. 12), it is possible to distinguish two periods during which processed anthropogenic continental air masses reached the site (between 19 and 24 July and between 30 July and 3 August 2013). The first period is characterized by high contributions of anthropogenic and oxygenated gas PMF factors (middle panel of Fig. 12) and an aerosol with inorganic (ammonium sulfate) and organic fractions in approximately similar proportions (top panel of Fig. 12). This period also corresponds to the highest values of ln(propane / ethane) of -1.4 on average and up to -0.8 (see bottom panel of Fig. 12); hence the less-aged air masses coinciding with the Europe northeast sector. The evolution of aerosol components and VOC factors during this period is also similar to that observed for the calm low wind conditions at the beginning of the campaign. These similarities could be related to the recirculation of air masses already observed in the western Mediterranean Basin, causing the formation of reservoir layers at high altitudes described in several studies (Pey et al., 2009; Minguillón et al., 2015; Ripoll et al., 2015).

The second period of long-range transported anthropogenic continental emissions is characterized by less intense anthropogenic gas-phase PMF factors, especially for the long-lived anthropogenic factor, and a clear predominance of the organic fraction for aerosols. Aerosol mass concentrations are also lower by approximately 50 % compared to the first period. During both periods, a non-negligible biogenic influence is also observed from primary and secondary biogenic PMF VOC factors. This is even more pronounced for the second "anthropogenic" period. During these periods, it is therefore likely that oxygenated VOCs and OOAs have both biogenic and anthropogenic origins in variable proportions.

A period of intense biogenic influence without significant long-range transport of anthropogenic continental emissions can also be distinguished (between 26 and 28 July) with elevated contributions of the primary and secondary biogenic

gas-phase PMF factors (Fig. 12). The oxygenated gas-phase PMF factor also rose during this period, and the aerosol composition is dominated by OA with low levels of inorganic aerosols. The inorganic fraction of aerosols decreases to reach less than 10 % of the aerosol composition on 27 July. This strong decrease occurred at the same time as a change in air mass origin from marine west to Corsica south. This is consistent with the lack of anthropogenic influence during this period, confirmed by lower ln(propane / ethane) of -1.8 on average up to -2.3 (see bottom panel of Fig. 12). It is therefore likely that the oxygenated VOCs and the organic fraction of aerosols during these days are mainly influenced by biogenic sources.

Finally, very low contributions of HOA were observed during the whole campaign from the PMF analysis of ACSM measurements (typically below 0.3 $\mu g\,m^{-3}$). This illustrates the weak influence of freshly emitted primary anthropogenic sources of OA at the site. This is also confirmed by low levels of black carbon (BC $< 0.9\,\mu g\,m^{-3}$ for the whole campaign; see Fig. 11a).

An analysis of the isotopic ratio of ^{14}C in aerosol sampled at Cape Corse reveals that the organic fraction of the aerosol measured during the ChArMEx SOP2 field campaign mainly came from biogenic sources and the oxidation of biogenic VOCs with a measured nonfossil OC of $2.42 \pm 0.86\,\mu gC\,m^{-3}$ on average (76 ± 3 % of OC on average). The secondary and primary anthropogenic sources to OC represented by measured fossil OC was $0.44 \pm 0.22\,\mu gC\,m^{-3}$ on average with a contribution to OC of 14 ± 3 % for OC on average. Elementary carbon contributed only 10 % of total carbon during the campaign with an average measured biomass EC and fossil EC of 0.16 ± 0.06 and $0.17 \pm 0.06\,\mu gC\,m^{-3}$, respectively. The results from this analysis will be presented in more detail in a forthcoming paper (Pey et al., 2017).

Given the good correlation observed between OA and the gas-phase oxygenated factor ($R^2 = 0.58$, $n = 498$), a common origin can be attributed to both OA and OVOCs observed at Cape Corse. A predominance of secondary biogenic origin during the whole campaign is likely for OVOCs, such as acetone, methanol and carboxylic acids, which composed the oxygenated PMF factor. As stated previously, this is also consistent with the large fraction of WSOC in OA, the fraction of which usually refers to biogenic SOA. A less important but still significant secondary anthropogenic origin is also likely for OVOCs.

5 Conclusions

The ChArMEx SOP2 field campaign provided a unique opportunity for insight into the various sources and fates of organic carbon in the Mediterranean atmosphere, thanks to the measurement of a large panel of gaseous and aerosol species at a remote site located at Cape Corse in the western Mediterranean Basin. The combination of gaseous and particulate organic databases, as collected during this campaign, is not common and has the potential to help improve our understanding of SOA formation. Moreover, the Mediterranean basin is an ideal location to characterize organics in the atmosphere since it is impacted by strong natural and anthropogenic sources and undergoes intense photochemical aging, especially during summer. The measurement site (Cape Corse) offered ideal experimental conditions since it is surrounded by the sea and is located at various distances from regional anthropogenic emission hot spots (such as north of Italy, southeast of France, northeast of Spain or north of Africa). These characteristics coupled with extremely low local anthropogenic sources allowed for the study of anthropogenic plumes after several days of atmospheric processing. In addition, intense local biogenic emissions permitted the investigation of biogenic and anthropogenic interactions in air mass composition.

These specific conditions led to the observation of contrasting situations, i.e., highly variable photochemical ages of processed anthropogenic air masses coupled with intense and local biogenic emissions. Low levels of anthropogenic VOCs (< 250 ppt for acetylene, for example) were observed overall, confirming the remoteness of the site. In contrast, significant levels of short-lived biogenic VOCs (up to 1.2 and 2.0 ppb for isoprene and the sum of monoterpenes, respectively) were observed. Elevated mixing ratios of OVOCs (e.g., up to 3.8 ppb for acetone) were also measured during the campaign due to the oxidation of both biogenic and anthropogenic precursors. These OVOCs exhibit the largest contribution to the VOC budget.

The aerosol chemical composition derived from Q-ACSM measurements shows a clear predominance of OM, which represents 55 % of the total mass of NR-PM_1 on average, followed by sulfate (27 %), ammonium (13 %) and nitrate (5 %). Furthermore, the temporal variability in OC and WSOC shows very similar patterns, leading to a clear linear correlation between the two datasets ($r^2 = 0.68$). The slope found is 0.58, highlighting that more than half of OC is water soluble.

PMF was conducted to identify covariation factors of VOCs that are representative of primary emissions and secondary photochemical transformations occurring during the transport of air masses. This analysis was performed using a gas-phase database of 42 VOCs (or sum of VOCs) of anthropogenic and biogenic origins, including NMHCs and OVOCs for the first time. A six-factor solution turned out to be optimal for this PMF analysis. In parallel, a concentration field (CF) analysis was conducted on four PMF factors to help in their identification through the localization of potential source areas. This combination of CF and PMF was particularly helpful in interpreting the factors associated with the long-range transport of anthropogenic compounds.

Three anthropogenic factors characterized by primary anthropogenic VOCs with various lifetimes were found. The CF analysis confirmed the anthropogenic nature of these fac-

tors by an identification of potential source areas in regions experiencing intense anthropogenic activities (e.g., the Po Valley and southeast of France).

Two biogenic factors were also identified. Both factors exhibited clear diurnal cycles and were correlated with temperature. In addition to a primary biogenic factor usually observed in VOC source apportionment studies, we also clearly identified, for the first time in PMF analysis, a secondary biogenic factor made up of first-generation oxidation products of biogenic VOCs.

A last oxygenated factor characterized by OVOCs of both biogenic and anthropogenic origins was also derived from the PMF analysis. The identification of this unusual factor was made possible by the extension of the input database to secondary oxygenated VOCs. This factor was influenced by anthropogenic and biogenic sources, showing elevated levels during periods of intense local biogenic influence (e.g., 26–28 July) and periods of long-range transport of anthropogenic continental emissions (e.g., 21–23 July). This factor was also correlated with submicron OA measured by ACSM ($R^2 = 0.58$, $n = 498$), highlighting the close link between secondary OVOCs and (secondary) OA at Cape Corse. The CF analysis of this factor suggested potential source areas that could be attributed to anthropogenic continental (north of Italy) and biogenic influences (areas in the south of Corsica).

The source apportionment of OA measured by ACSM led to a three-factor solution identified as hydrogen-like OA, semi-volatile oxygenated OA and low volatility oxygenated OA. These three factors accounted for an averaged mass concentration of 0.13, 1.59 and 1.92 $\mu g\,m^{-3}$, respectively, for a total OA mass concentration of 3.63 $\mu g\,m^{-3}$, mainly associated with secondary formation (96 %).

A coupled analysis of VOC and OA sources was conducted. During biogenic periods, the aerosol composition was dominated by (secondary) OA, indicating a substantial impact of BVOCs on aerosol composition. During periods of long-range transport of anthropogenic continental emissions, the inorganic and organic fractions of submicron aerosols were similar. During the whole campaign, low levels of hydrogen-like OA (HOA) were observed ($< 0.3\,\mu g\,m^{-3}$), indicating a weak influence of primary anthropogenic sources on OA.

Data availability. Access to the data used for this publication is restricted to registered users following the data and publication policy of the ChArMEx program (http://mistrals.sedoo.fr/ChArMEx/Data-Policy/ChArMEx_DataPolicy.pdf).

The Supplement related to this article is available online at https://doi.org/10.5194/acp-17-8837-2017-supplement.

Competing interests. The authors declare that they have no conflict of interest.

Special issue statement. This article is part of the special issue "CHemistry and AeRosols Mediterranean EXperiments (ChArMEx; ACP/AMT inter-journal SI)". It does not belong to a conference.

Acknowledgements. This study received financial support from the MISTRALS and ChArMEx programs, ADEME, the French Environmental Ministry, the CaPPA projects and the Communauté Territoriale de Corse (CORSiCA project). The CaPPA project (Chemical and Physical Properties of the Atmosphere) is funded by the French National Research Agency (ANR) through the PIA (Programme d'Investissement d'Avenir) under contract ANR-11-LABX-0005-01 and by the Regional Council Nord-Pas de Calais and the European Funds for Regional Economic Development (FEDER). This research was also funded by the European Union Seventh Framework Programme under grant agreement number 293897, the DEFI-VOC project, CARBO-SOR/Primequal and SAF-MED (ANR grant number ANR-12-BS06-0013-02). Greenhouse gas data were provided by the ICOS France monitoring network.

The authors also want to thank Eric Hamonou and François Dulac for logistical help during the campaign and all the participants of the ChArMEx SOP2 field campaign.

Edited by: Nikolaos Mihalopoulos
Reviewed by: three anonymous referees

References

ACTRIS Measurement Guideline VOC: WP4- NA4: Trace gases networking: Volatile organic carbon and nitrogen oxidesDeliverable D4.9: Final SOPs for VOCs measurements, 25–28, http://www.actris.eu/Portals/46/DataandServices/Measurementguidelines/Near-surfacetracegases/ACTRIS-1Deliverable_WP4_D4.9_M42_v2_Sep2014.pdf?ver=2017-03-20-135044- (last access: 6 July 2017), 2014.

Aiken, A. C., DeCarlo, P. F., Kroll, J. H., Worsnop, D. R., Huffman, J. A., Docherty, K. S., Ulbrich, I. M., Mohr, C., Kimmel, J. R., Sueper, D., Sun, Y., Zhang, Q., Trimborn, A., Northway, M., Ziemann, P. J., Canagaratna, M. R., Onasch, T. B., Alfarra, M. R., Prevot, A. S. H., Dommen, J., Duplissy, J., Metzger, A., Baltensperger, U., and Jimenez, J. L.: O / C and OM / OC ratios of primary, secondary, and ambient organic aerosols with high-resolution time-of-flight aerosol mass spectrometry, Environ. Sci. Technol., 42, 4478–4485, 2008.

Ait-Helal, W., Borbon, A., Sauvage, S., de Gouw, J. A., Colomb, A., Gros, V., Freutel, F., Crippa, M., Afif, C., Baltensperger, U., Beekmann, M., Doussin, J.-F., Durand-Jolibois, R., Fronval, I., Grand, N., Leonardis, T., Lopez, M., Michoud, V., Miet, K., Perrier, S., Prévôt, A. S. H., Schneider, J., Siour, G., Zapf, P., and Locoge, N.: Volatile and intermediate volatility organic compounds in suburban Paris: variability, origin and importance

for SOA formation, Atmos. Chem. Phys., 14, 10439–10464, https://doi.org/10.5194/acp-14-10439-2014, 2014.

Ashbaugh, L. L., Malm, W. C., and Sadeh, W. Z.: A residence time probability analysis of sulfur concentrations at grand-canyonnational-park, Atmos. Environ., 19, 1263–1270, 1985.

Atkinson, R.: Atmospheric chemistry of VOCs and NO_x, Atmos. Environ., 34, 2063–2101, https://doi.org/10.1016/s1352-2310(99)00460-4, 2000.

Aumont, B., Szopa, S., and Madronich, S.: Modelling the evolution of organic carbon during its gas-phase tropospheric oxidation: development of an explicit model based on a self generating approach, Atmos. Chem. Phys., 5, 2497–2517, https://doi.org/10.5194/acp-5-2497-2005, 2005.

Aumont, B., Valorso, R., Mouchel-Vallon, C., Camredon, M., Lee-Taylor, J., and Madronich, S.: Modeling SOA formation from the oxidation of intermediate volatility *n*-alkanes, Atmos. Chem. Phys., 12, 7577–7589, https://doi.org/10.5194/acp-12-7577-2012, 2012.

Badol, C., Borbon, A., Locoge, N., Leonardis, T., and Galloo, J. C.: An automated monitoring system for VOC ozone precursors in ambient air: development, implementation and data analysis, Anal. Bioanal. Chem., 378, 7, 1815–1827, 2004.

Bae, M.-S., Schauer, J. J., DeMinter, J. T., Turner, J. R., Smith, D., and Cary, R. A.: Validation of a semi-continuous instrument for elemental carbon and organic carbon using a thermal-optical method, Atmos. Environ., 38, 2885–2893, 2004.

Budisulistiorini, S. H., Baumann, K., Edgerton, E. S., Bairai, S. T., Mueller, S., Shaw, S. L., Knipping, E. M., Gold, A., and Surratt, J. D.: Seasonal characterization of submicron aerosol chemical composition and organic aerosol sources in the southeastern United States: Atlanta, Georgia,and Look Rock, Tennessee, Atmos. Chem. Phys., 16, 5171–5189, https://doi.org/10.5194/acp-16-5171-2016, 2016.

Canagaratna, M. R., Jayne, J. T., Ghertner, D. A., Herndon, S., Shi, Q., Jimenez, J. L., Silva, P. J., Williams, P., Lanni, T., Drewnick, F., Demerjian, K. L., Kolb, C. E., and Worsnop, D. R.: Chase studies of particulate emissions from in-use New York City vehicles, Aerosol Sci. Tech., 38, 555–573, 2004.

Canonaco, F., Crippa, M., Slowik, J. G., Baltensperger, U., and Prévôt, A. S. H.: SoFi, an IGOR-based interface for the efficient use of the generalized multilinear engine (ME-2) for the source apportionment: ME-2 application to aerosol mass spectrometer data, Atmos. Meas. Tech., 6, 3649–3661, https://doi.org/10.5194/amt-6-3649-2013, 2013.

Carlton, A. G., Turpin, B. J., Altieri, K. E., Seitzinger, S., Reff, A., Lim, H. J., and Ervens, B.: Atmospheric oxalic acid and SOA production from glyoxal: Results of aqueous photooxidation experiments, Atmos. Environ., 41, 7588–7602, 2007.

CCI Territorial Bastia Haute Corse: Port de Bastia Statistiques Portuaires 2013, http://www.bastia-hautecorse.cci.fr/PortBia/images/stats/annuel_2014_bastia_2013.pdf (last access: 16 July 2017), 2013.

Charron, A., Plaisance, H., Sauvage, S., Coddeville, P., Galoo, J. C., and Guillermo, R.: A study of the sourceereceptor relationships influencing the acidity of precipitation collected at a rural site in France, Atmos. Environ., 34, 3665–3674, 2000.

Chirico, R., DeCarlo, P. F., Heringa, M. F., Tritscher, T., Richter, R., Prévôt, A. S. H., Dommen, J., Weingartner, E., Wehrle, G., Gysel, M., Laborde, M., and Baltensperger, U.: Impact of aftertreatment devices on primary emissions and secondary organic aerosol formation potential from in-use diesel vehicles: results from smog chamber experiments, Atmos. Chem. Phys., 10, 11545–11563, https://doi.org/10.5194/acp-10-11545-2010, 2010.

Crahan, K. K., Hegg, D., Covert, D. S., and Jonsson, H.: An exploration of aqueous oxalic acid production in the coastal marine atmosphere, Atmos. Environ., 38, 3757–3764, 2004.

Crenn, V., Sciare, J., Croteau, P. L., Verlhac, S., Fröhlich, R., Belis, C. A., Aas, W., Äijälä, M., Alastuey, A., Artiñano, B., Baisnée, D., Bonnaire, N., Bressi, M., Canagaratna, M., Canonaco, F., Carbone, C., Cavalli, F., Coz, E., Cubison, M. J., Esser-Gietl, J. K., Green, D. C., Gros, V., Heikkinen, L., Herrmann, H., Lunder, C., Minguillón, M. C., Močnik, G., O'Dowd, C. D., Ovadnevaite, J., Petit, J.-E., Petralia, E., Poulain, L., Priestman, M., Riffault, V., Ripoll, A., Sarda-Estève, R., Slowik, J. G., Setyan, A., Wiedensohler, A., Baltensperger, U., Prévôt, A. S. H., Jayne, J. T., and Favez, O.: ACTRIS ACSM intercomparison – Part 1: Reproducibility of concentration and fragment results from 13 individual Quadrupole Aerosol Chemical Speciation Monitors (Q-ACSM) and consistency with co-located instruments, Atmos. Meas. Tech., 8, 5063–5087, https://doi.org/10.5194/amt-8-5063-2015, 2015.

Crippa, M., Canonaco, F., Slowik, J. G., El Haddad, I., DeCarlo, P. F., Mohr, C., Heringa, M. F., Chirico, R., Marchand, N., Temime-Roussel, B., Abidi, E., Poulain, L., Wiedensohler, A., Baltensperger, U., and Prévôt, A. S. H.: Primary and secondary organic aerosol origin by combined gas-particle phase source apportionment, Atmos. Chem. Phys., 13, 8411–8426, https://doi.org/10.5194/acp-13-8411-2013, 2013a.

Crippa, M., El Haddad, I., Slowik, J. G., DeCarlo, P. F., Mohr, C., Heringa, M. F., Chirico, R., Marchand, N., Sciare, J., Baltensperger, U., and Prévôt, A. S. H.: Identification of marine and continental aerosol sources in Paris using high resolution aerosol mass spectrometry, J. Geophys. Res.-Atmos., 118, 1950–1963, 2013b.

de Angelis, M., Traversi, R., and Udisti, R.: Long-term trends of mono-carboxylic acids in Antarctica: comparison of changes in sources and transport processes at the two EPICA deep drilling sites, Tellus B, 64, 17331, https://doi.org/10.3402/tellusb.v64i0.17331, 2012.

Debevec, C., Sauvage, S., Gros, V., Sciare, J., Pikridas, M., Stavroulas, I., Salameh, T., Leonardis, T., Gaudion, V., Depelchin, L., Fronval, I., Sarda-Esteve, R., Baisnée, D., Bonsang, B., Savvides, C., Vrekoussis, M., and Locoge, N.: Origin and variability of volatile organic compounds observed at an Eastern Mediterranean background site (Cyprus), Atmos. Chem. Phys. Discuss., https://doi.org/10.5194/acp-2016-1178, in review, 2017.

de Gouw, J. and Warneke, C.: Measurements of volatile organic compounds in the earth's atmosphere using proton-transferreaction mass spectrometry, Mass. Spectrom. Rev., 26, 223–257, https://doi.org/10.1002/mas.20119, 2007.

Detournay, A., Sauvage, S., Locoge, N., Gaudion, V., Leonardis, T., Fronval, I., Kaluzny, P., and Galloo, J.-C.: Development of a sampling method for the simultaneous monitoring of straightchain alkanes, straight-chain saturated carbonyl compounds and monoterpenes in remote areas, J. Environ. Monit., 13, 983–990, 2011.

Draxler, R. R. and Hess, G. D.: An overview of the HYSPLIT 4 modeling system for trajectories, dispersion, and deposition, Aust. Meteorol. Mag., 47, 295–308, 1998.

Ervens, B., Feingold, G., Frost, G. J., and Kreidenweis, S. M.: A modeling study of aqueous production of dicarboxylic acids: 1. Chemical pathways and speciated organic mass production, J. Geophys. Res.-Atmos., 109, D15205, https://doi.org/10.1029/2003JD004387, 2004.

Ervens, B., Carlton, A. G., Turpin, B. J., Altieri, K. E., Kreidenweis, S. M., and Feingold, G.: Secondary organic aerosol yields from cloud-processing of isoprene oxidation products, Geophys. Res. Lett., 35, L02816, https://doi.org/10.1029/2007GL031828, 2008.

Eyring, V., Kohler, H. W., van Aardenne, J., and Lauer, A.: Emissions from international shipping: 1. The last 50 years, J. Geophys. Res., 110, D17305, https://doi.org/10.1029/2004JD005619, 2005.

Fares, S., Park, J. H., Gentner, D. R., Weber, R., Ormeno, E., Karlik, J., and Goldstein, A. H.: Seasonal cycles of biogenic volatile organic compound fluxes and concentrations in a California citrus orchard, Atmos. Chem. Phys., 12, 9865–9880, https://doi.org/10.5194/acp-12-9865-2012, 2012.

Forster, P., Ramaswamy, V., Artaxo, P., Berntsen, T., Betts, R., Fahey, D. W., Haywood, J., Lean, J., Lowe, D. C., Myhre, G., Nganga, J., Prinn, R., Raga, G., Schulz, M., and Van Dorland, R.: Radiative Forcing of Climate Change, in: Climate Change 2007: The Physical Science Basis, Contribution of Working Group I to the Fourth Assessment Report of the Intergovernmental Panel on Climate Change, edited by: Solomon, S., Qin, D., Manning, M., Chen, Z., Marquis, M., Averyt, K. B., Tignor, M., and Miller, H. L., Cambridge University Press, Cambridge, United Kingdom and New York, NY, USA, 2007.

Fröhlich, R., Crenn, V., Setyan, A., Belis, C. A., Canonaco, F., Favez, O., Riffault, V., Slowik, J. G., Aas, W., Aijälä, M., Alastuey, A., Artiñano, B., Bonnaire, N., Bozzetti, C., Bressi, M., Carbone, C., Coz, E., Croteau, P. L., Cubison, M. J., Essergietl, J. K., Green, D. C., Gros, V., Heikkinen, L., Herrmann, H., Jayne, J. T., Lunder, C. R., Minguillón, M. C., Mocnik, G., O'Dowd, C. D., Ovadnevaite, J., Petralia, E., Poulain, L., Priestman, M., Ripoll, A., Sarda-Estève, R., Wiedensohler, A., Baltensperger, U., Sciare, J., and Prévôt, A. S. H.: ACTRIS ACSM intercomparison – Part 2: Intercomparison of ME-2 organic source apportionment results from 15 individual, co-located aerosol mass spectrometers, Atmos. Meas. Tech., 8, 2555–2576, https://doi.org/10.5194/amt-8-2555-2015, 2015.

Fu, T. M., Jacob, D. J., Wittrock, F., Burrows, J. P., Vrekoussis, M., and Henze, D. K., Global budgets of atmospheric glyoxal and methylglyoxal, and implications for formation of secondary organic aerosols, J. Geophys. Res.-Atmos., 113, D15303, https://doi.org/10.1029/2007JD009505, 2008.

Gaimoz, C., Sauvage, S., Gros, V., Herrmann, F., Williams, J., Locoge, N., Perrussel, O., Bonsang, B., d'Argouges, O., SardaEsteve, R., and Sciare, J.: Volatile Organic Compounds sources in Paris in spring 2007, Part II: Source apportionment using positive matrix factorisation, Environ. Chem., 8, 91–103, https://doi.org/10.1071/en10067, 2011.

Goldstein, A. H. and Galbally, I. E.: Known and unexplored organic constituents in the earth's atmosphere, Environ. Sci. Technol., 41, 1514–1521, 2007.

Goldstein, A. H. and Schade, G. W.: Quantifying biogenic and anthropogenic contributions to acetone mixing ratios in a rural environment, Atmos. Environ., 34, 4997–5006, 2000.

Guenther, A., Hewitt, C. N., Erickson, D., Fall, R., Geron, C., Graedel, T., Harley, P., Klinger, L., Lerdau, M., McKay, W. A., Pierce, T., Scholes, B., Steinbrecher, R., Tallamraju, R., Taylor, J., and Zimmerman, P.: A global model of natural volatile organic compound emissions, J. Geophys. Res., 100, 8873–8892, 1995.

Guenther, A., Geron, C., Pierce, T., Lamb, B., Harley, P., and Fall, R.: Natural emissions of non-methane volatile organic compounds, carbon monoxide, and oxides of nitrogen from North America, Atmos. Environ., 34, 2205–2230, 2000.

Heald, C. L., Jacob, D. J., Turquety, S., Hudman, R. C., Weber, R. J., Sullivan, A. P., Peltier, R. E., Atlas, E. L., de Gouw, J. A., Warneke, C., Holloway, J. S., Neuman, J. A., Flocke, F. M., and Seinfeld, J. H.: Concentrations and sources of organic carbon aerosols in the free troposphere over North America, J. Geophys. Res., 111, D23S47, https://doi.org/10.1029/2006JD007705, 2006.

Hennigan, C. J., Bergin, M. H., Dibb, J. E., and Weber, R. J.: Enhanced secondary organic aerosol formation due to water uptake by fine particles, Geophys. Res. Lett., 35, L18801, https://doi.org/10.1029/2008GL035046, 2008a.

Hennigan, C. J., Bergin, M. H., and Weber, R. J.: Correlations between water-soluble organic aerosol and water vapor: a synergistic effect from biogenic emissions?, Environ. Sci Technol., 42, 9079–9085, 2008b.

Hildebrandt, L., Engelhart, G. J., Mohr, C., Kostenidou, E., Lanz, V. A., Bougiatioti, A., DeCarlo, P. F., Prevot, A. S. H., Baltensperger, U., Mihalopoulos, N., Donahue, N. M., and Pandis, S. N.: Aged organic aerosol in the Eastern Mediterranean: the Finokalia Aerosol Measurement Experiment – 2008, Atmos. Chem. Phys., 10, 4167–4186, https://doi.org/10.5194/acp-10-4167-2010, 2010.

Holzinger, R., Warneke, C., Hansel, A., Jordan, A., Lindinger, W., Scharffe, D. H., Schade, G., and Crutzen, P. J.: Biomass burning as a source of formaldehyde, acetaldehyde, methanol, acetone, acetonitrile, and hydrogen cyanide, Geophys. Res. Lett., 26, 1161–1164, https://doi.org/10.1029/1999GL900156, 1999.

Holzinger, R., Lee, A., Paw, K. T., and Goldstein, U. A. H.: Observations of oxidation products above a forest imply biogenic emissions of very reactive compounds, Atmos. Chem. Phys., 5, 67–75, https://doi.org/10.5194/acp-5-67-2005, 2005.

Hopke, P. K.: A Guide to Positive Matrix Factorization, EPA Workshop Proceedings, Materials from the Workshop on UNMIX and PMF as Applied to $PM_{2.5}$, 14–16 February 2000, Research Triangle Park, North Carolina, USA, 2000.

Hopke, P. K.: Recent developments in receptor modeling, J. Chemometr., 17, 255–265, https://doi.org/10.1002/cem.796, 2003.

Hu, L., Millet, D. B., Mohr, M. J., Wells, K. C., Griffis, T. J., and Helmig, D.: Sources and seasonality of atmospheric methanol based on tall tower measurements in the US Upper Midwest, Atmos. Chem. Phys., 11, 11145–11156, https://doi.org/10.5194/acp-11-11145-2011, 2011.

Hu, L., Millet, D. B., Kim, S. Y., Wells, K. C., Griffis, T. J., Fischer, E. V., Helmig, D., Hueber, J., and Curtis, A. J.: North American acetone sources determined from tall tower measure-

ments and inverse modeling, Atmos. Chem. Phys., 13, 3379–3392, https://doi.org/10.5194/acp-13-3379-2013, 2013.

Huang, X. F. and Yu, J. Z., Is vehicle exhaust a significant primary source of oxalic acid in ambient aerosols?, Geophys. Res. Lett., 34, L02808, https://doi.org/10.1029/2006GL028457, 2007.

Hwang, I. and Hopke, P. K.: Estimation of source apportionment and potential source locations of $PM_{2.5}$ at a west coastal IMPROVE site, Atmos. Environ., 41, 506–518, 2007.

Jimenez, J. L., Canagaratna, M. R., Donahue, N. M., Prevot, A. S. H., Zhang, Q., Kroll, J. H., DeCarlo, P. F., Allan, J. D., Coe, H., Ng, N. L., Aiken, A. C., Docherty, K. S., Ulbrich, I. M., Grieshop, A. P., Robinson, A. L., Duplissy, J., Smith, J. D., Wilson, K. R., Lanz, V. A., Hueglin, C., Sun, Y. L., Tian, J., Laaksonen, A., Raatikainen, T., Rautiainen, J., Vaattovaara, P., Ehn, M., Kulmala, M., Tomlinson, J. M., Collins, D. R., Cubison, M. J., Dunlea, E. J., Huffman, J. A., Onasch, T. B., Alfarra, M. R., Williams, P. I., Bower, K., Kondo, Y., Schneider, J., Drewnick, F., Borrmann, S., Weimer, S., Demerjian, K., Salcedo, D., Cottrell, L., Griffin, R., Takami, A., Miyoshi, T., Hatakeyama, S., Shimono, A., Sun, J. Y., Zhang, Y. M., Dzepina, K., Kimmel, J. R., Sueper, D., Jayne, J. T., Herndon, S. C., Trimborn, A. M., Williams, L. R., Wood, E. C., Middlebrook, A. M., Kolb, C. E., Baltensperger, U., and Worsnop, D. R.: Evolution of Organic Aerosols in the Atmosphere, Science, 326, 1525–1529, 2009.

Jobson, B. T., Wu, Z., Niki, H., and Barrie, L. A.: Seasonal trends of isoprene, C_2–C_5 alkanes, and acetylene at a remote boreal site in Canada, J. Geophys. Res., 99, 1589–1599, 1994.

Kanakidou, M., Seinfeld, J. H., Pandis, S. N., Barnes, I., Dentener, F. J., Facchini, M. C., Van Dingenen, R., Ervens, B., Nenes, A., Nielsen, C. J., Swietlicki, E., Putaud, J. P., Balkanski, Y., Fuzzi, S., Horth, J., Moortgat, G. K., Winterhalter, R., Myhre, C. E. L., Tsigaridis, K., Vignati, E., Stephanou, E. G., and Wilson, J.: Organic aerosol and global climate modelling: a review, Atmos. Chem. Phys., 5, 1053–1123, https://doi.org/10.5194/acp-5-1053-2005, 2005.

Kawamura, K., Kasukabe, H., and Barrie, L. A.: Source and reaction pathways of dicarboxylic acids, ketoacids and dicarbonyls in arctic aerosols: One year of observations, Atmos. Environ., 30, 1709–1722, 1996.

Kondo, Y., Miyazaki, Y., Takegawa, N., Miyakawa, T., Weber, R. J., Jimenez, J. L., Zhang, Q., and Worsnop, D. R.: Oxygenated and water-soluble organic aerosols in Tokyo, J. Geophys. Res., 112, D01203, https://doi.org/10.1029/2006jd007056, 2007.

Kroll, J. H. and Seinfeld, J. H.: Chemistry of secondary organic aerosol: Formation and evolution of low-volatility organics in the atmosphere, Atmos. Environ., 42, 3593–3624, 2008.

Lanz, V. A., Henne, S., Staehelin, J., Hueglin, C., Vollmer, M. K., Steinbacher, M., Buchmann, B., and Reimann, S.: Statistical analysis of anthropogenic non-methane VOC variability at a European background location (Jungfraujoch, Switzerland), Atmos. Chem. Phys., 9, 3445–3459, https://doi.org/10.5194/acp-9-3445-2009, 2009.

Latella, A., Stani, G., Cobelli, L., Duane, M., Junninen, H., Astorga, C., and Larsen, B. R.: Semicontinuous GC analysis and receptor modelling for source apportionment of ozone precursor hydrocarbons in Bresso, Milan, 2003, J. Chromatr. A, 39, 29–39, 2005.

Lee, A., Goldstein, A. H., Keywood, M. D., Gao, S., Varutbangkul, V., Bahreini, R., Ng, N. L., Flagan, R. C., and Seinfeld, J. H.: Gas-phase products and secondary aerosol yields from the ozonolysis of ten different terpenes, J. Geophys. Res.-Atmos., 111, D07302, https://doi.org/10.1029/2005jd006437, 2006.

Lelieveld, J., Berresheim, H., Borrmann, S., Crutzen, P. J., Dentener, F. J., Fischer, J., Flatau, P. J., Heland, J., Holzinger, R., Korrmann, R., Lawrence, M. G., Levi, Z., Markowicz, K. M., Mihalopoulos, N., Minikin, A., Ramanathan, V., De Reus, M., Roelofs, G. J., Scheeren, H. A., Sciare, J., Schlager, H., Schultz, M., Seigmund, P., Steil, B., Stephanou, E. G., Steir, P., Traub, M., Warneke, C., Williams, J., and Ziereis, H.: Global air pollution crossroads over the Mediterranean, Science, 298, 794–799, 2002.

Leuchner, M. and Rappenglück, B.: VOC source–receptor relationships in Houston during TexAQS-II, Atmos. Environ., 44, 4056–4067, https://doi.org/10.1016/j.atmosenv.2009.02.029, 2010.

Leuchner, M., Gubo, S., Schunk, C., Wastl, C., Kirchner, M., Menzel, A., and Plass-Dülmer, C.: Can positive matrix factorization help to understand patterns of organic trace gases at the continental Global Atmosphere Watch site Hohenpeissenberg?, Atmos. Chem. Phys., 15, 1221–1236, https://doi.org/10.5194/acp-15-1221-2015, 2015.

Lim, H. J., Carlton, A. G., and Turpin, B. J.: Isoprene forms secondary organic aerosol through cloud processing: Model simulations, Environ. Sci. Technol., 39, 4441–4446, 2005.

Lohmann, U. and Feichter, J.: Global indirect aerosol effects: a review, Atmos. Chem. Phys., 5, 715–737, https://doi.org/10.5194/acp-5-715-2005, 2005.

MacDonald, R. C. and Fall, R.: Detection of substantial emissions of methanol from plants to the atmosphere, Atmos. Environ., 27, 1709–1713, https://doi.org/10.1016/0960-1686(93)90233-O, 1993.

Madronich, S.: Chemical evolution of gaseous air pollutants downwind of tropical megacities: Mexico City case study, Atmos. Environ., 40, 6012–6018, https://doi.org/10.1016/j.atmosenv.2005.08.047, 2006.

McKeen, S. A., Liu, S. C., Hsie, E.-Y., Lin, X., Bradshaw, J. D., Smyth, S., Gregory, G. L., and Blake, D. R.: Hydrocarbon ratios during PEM-WEST A: a model perspective, J. Geophys. Res., 101, 2087–2109, https://doi.org/10.1029/95JD02733, 1996.

Minguillón, M. C., Ripoll, A., Pérez, N., Prévôt, A. S. H., Canonaco, F., Querol, X., and Alastuey, A.: Chemical characterization of submicron regional background aerosols in the western Mediterranean using an Aerosol Chemical Speciation Monitor, Atmos. Chem. Phys., 15, 6379–6391, https://doi.org/10.5194/acp-15-6379-2015, 2015.

Minguillón, M. C., Pérez, N., Marchand, N., Bertrand, A., TemimeRoussel, B., Agrios, K., Szidat, S., van Drooge, B. L., Sylvestre, A., Alastuey, A., Reche, C., Ripoll, A., Marco, E., Grimalt, J. O., and Querol, X.: Secondary organic aerosol origin in an urban environment. Influence of biogenic and fuel combustion precursors, Faraday Discuss., 189, 337–359, https://doi.org/10.1039/c5fd00182j, 2016.

Miyazaki, Y., Kondo, Y., Takegawa, N., Komazaki, Y., Fukuda, M., Kawamura, K., Mochida, M., Okuzawa, K., and Weber, R. J.: Time-resolved measurements of water-soluble organic carbon in Tokyo, J. Geophys. Res., 111, D23206, https://doi.org/10.1029/2006jd007125, 2006.

Miyoshi, A., Hatakeyama, S., and Washida, N.: OH radical-initiated photooxidation of isoprene: an estimate of global CO production, J. Geophys. Res.-Atmos., 99, 18779–18787, 1994.

Mohr, C., DeCarlo, P. F., Heringa, M. F., Chirico, R., Slowik, J. G., Richter, R., Reche, C., Alastuey, A., Querol, X., Seco, R., Peñuelas, J., Jiménez, J. L., Crippa, M., Zimmermann, R., Baltensperger, U., and Prévôt, A. S. H.: Identification and quantification of organic aerosol from cooking and other sources in Barcelona using aerosol mass spectrometer data, Atmos. Chem. Phys., 12, 1649–1665, https://doi.org/10.5194/acp-12-1649-2012, 2012.

Myriokefalitakis, S., Tsigaridis, K., Mihalopoulos, N., Sciare, J., Nenes, A., Kawamura, K., Segers, A., and Kanakidou, M.: In-cloud oxalate formation in the global troposphere: a 3-D modeling study, Atmos. Chem. Phys., 11, 5761–5782, https://doi.org/10.5194/acp-11-5761-2011, 2011.

Ng, N. L., Canagaratna, M. R., Zhang, Q., Jimenez, J. L., Tian, J., Ulbrich, I. M., Kroll, J. H., Docherty, K. S., Chhabra, P. S., Bahreini, R., Murphy, S. M., Seinfeld, J. H., Hildebrandt, L., Donahue, N. M., DeCarlo, P. F., Lanz, V. A., Prevôt, A. S. H., Dinar, E., Rudich, Y., and Worsnop, D. R.: Organic aerosol components observed in Northern Hemispheric datasets from Aerosol Mass Spectrometry, Atmos. Chem. Phys., 10, 4625–4641, https://doi.org/10.5194/acp-10-4625-2010, 2010a.

Ng, N. L., Canagaratna, M. R., Jimenez, J. L., Zhang, Q., Ulbrich, I. M., and Worsnop, D. R.: Real-time methods for estimating organic component mass concentrations from aerosol mass spectrometer data, Environ. Sci. Tech., 45, 910–916, 2010b.

Ng, N. L., Herndon, S. C., Trimborn, A., Canagaratna, M. R., Croteau, P. L., Onasch, T. B., Sueper, D., Worsnop, D. R., Zhang, Q., Sun, Y. L., and Jayne, J. T.: An Aerosol Chemical Speciation Monitor (ACSM) for Routine Monitoring of the Composition and Mass Concentrations of Ambient Aerosol, Aerosol Sci. Tech., 45, 780–794, https://doi.org/10.1080/02786826.2011.560211, 2011.

Orsini, D. A., Ma, Y., Sullivan, A., Sierau, B., Baumann, K., and Weber, R.: Refinements to the Particle-Into-Liquid Sampler (PILS) for ground and airborne measurements of water soluble aerosol composition, Atmos. Environ., 37, 1243–1259, 2003.

Paatero, P.: A weighted non-negative least squares algorithm for three-way "PARAFAC" factor analysis, Chemometr. Intel. Lab. Syst., 38, 223–242, 1997.

Paatero, P.: The multilinear engine – A table-driven, least squares program for solving multilinear problems, including the *n*-way parallel factor analysis model, J. Comp. Graph. Stat., 8, 854–888, https://doi.org/10.2307/1390831, 1999.

Paatero, P. and Tapper, U.: Positive MAtrix Factorization: a non-negative factor model with optimal utilization of error estimates of data values, Environmetrics, 5, 111–126, 1994.

Park, J.-H., Goldstein, A. H., Timkovsky, J., Fares, S., Weber, R., Karlik, J., and Holzinger, R.: Eddy covariance emission and deposition flux measurements using proton transfer reaction – time of flight – mass spectrometry (PTR-TOF-MS): comparison with PTR-MS measured vertical gradients and fluxes, Atmos. Chem. Phys., 13, 1439–1456, https://doi.org/10.5194/acp-13-1439-2013, 2013.

Parrish, D. D., Hahn, C. J., Williams, E. J., Norton, R. B., Fehsenfeld, F. C., Singh, H. B., Shetter, J. D., Gandrud, B. W., and Ridley, B. A.: Indications of photochemical histories of Pacific air masses from measurements of atmospheric trace species at Point Arena, California, J. Geophys. Res., 97, 15883–15901, 1992.

Parrish, D. D., Stohl, A., Forster, C., Atlas, E. L., Blake, D. R., Goldan, P. D., Kuster, W. C., and de Gouw, J. A.: Effects of mixing on evolution of hydrocarbon ratios in the troposphere, J. Geophys. Res.-Atmos., 112, D10S34, https://doi.org/10.1029/2006JD007583, 2007.

Parworth, C., Fast, J., Mei, F., Shippert, T., Sivaraman, C., Tilp, A., Watson, T., and Zhang, Q.: Long-term measurements of submicrometer aerosol chemistry at the Southern Great Plains (SGP) using an Aerosol Chemical Speciation Monitor (ACSM), Atmos. Environ., 106, 43–55, 2015.

Peltier, R. E., Weber, R. J., and Sullivan, A. P.: Investigating a Liquid-Based Method for Online Organic Carbon Detection in Atmospheric Particles, Aerosol Sci. Tech., 41, 1117–1127, https://doi.org/10.1080/02786820701777465, 2007.

Petit, J.-E., Favez, O., Sciare, J., Crenn, V., Sarda-Estève, R., Bonnaire, N., Mocnik, G., Dupont, J.-C., Haeffelin, M., and Leoz-Garziandia, E.: Two years of near real-time chemical composition of submicron aerosols in the region of Paris using an Aerosol Chemical Speciation Monitor (ACSM) and a multi-wavelength Aethalometer, Atmos. Chem. Phys., 15, 2985–3005, https://doi.org/10.5194/acp-15-2985-2015, 2015.

Pey, J., Pérez, N., Castillo, S., Viana, M., Moreno, T., Pandolfi, M., López-Sebastián, J. M., Alastuey, A., and Querol, X.: Geochemistry of regional background aerosols in the Western Mediterranean, Atmos. Res., 94, 422–435, 2009.

Pey, J., DeWitt, H. L., Cerro, J. C., Perez, N., Temime-Roussel, B., Elser, M., Hellebust, S., Sylvestre, A., Sartelet, K., Mocnik, G., Szidat, S., and Prévôt, A. S. H., Marchand N.: Sources and physico-chemical propreties of aerosols over western Mediterranean insular background environments in summer 2013.

Pope, C. A. and Dockery, D. W.: Health effects of fine particulate air pollution: Lines that connect, J. Air Waste Manage. Assoc., 56, 709–742, 2006.

Reissell, A., Harry, C., Aschmann, S. M., Atkinson, R., and Arey, J.: Formation of acetone from the OH radical- and O_3-initiated reactions of a series of monoterpenes, J. Geophys. Res., 104, 13869–13879, 1999.

Ripoll, A., Minguillón, M. C., Pey, J., Jimenez, J. L., Day, D. A., Sosedova, Y., Canonaco, F., Prévôt, A. S. H., Querol, X., and Alastuey, A.: Long-term real-time chemical characterization of submicron aerosols at Montsec (southern Pyrenees, 1570 m a.s.l.), Atmos. Chem. Phys., 15, 2935–2951, https://doi.org/10.5194/acp-15-2935-2015, 2015.

Roukos, J., Plaisance, H., Leonardis, T., Bates, M., and Locoge, N.: Development and validation of an automated monitoring system for oxygenated volatile organic compounds and nitrile compounds in ambient air, J. Chromatr. A, 1216, 8642–8651, https://doi.org/10.1016/j.chroma.2009.10.018, 2009.

Rudolph, J. and Johnen, F. J.: Measurements of light atmospheric hydrocarbons over the Atlantic in regions of low biological activity, J. Geophys. Res., 95, 20583–20591, https://doi.org/10.1029/JD095iD12p20583, 1990.

Sauvage, S., Plaisance, H., Locoge, N., Wroblewski, A., Coddeville, P., and Galloo, J. C.: Long term measurement and source apportionment of non-methane hydrocarbons in three French rural areas, Atmos. Environ., 43, 2430–2441, https://doi.org/10.1016/j.atmosenv.2009.02.001, 2009.

Sciare, J., Cachier, H., Oikonomou, K., Ausset, P., Sarda-Estève, R., and Mihalopoulos, N.: Characterization of carbona-

ceous aerosols during the MINOS campaign in Crete, July–August 2001: a multi-analytical approach, Atmos. Chem. Phys., 3, 1743–1757, https://doi.org/10.5194/acp-3-1743-2003, 2003.

Sciare, J., Oikonomou, K., Favez, O., Liakakou, E., Markaki, Z., Cachier, H., and Mihalopoulos, N.: Long-term measurements of carbonaceous aerosols in the Eastern Mediterranean: evidence of long-range transport of biomass burning, Atmos. Chem. Phys., 8, 5551–5563, https://doi.org/10.5194/acp-8-5551-2008, 2008.

Sciare, J., d'Argouges, O., Sarda-Esteve, R., Gaimoz, C., Dolgorouky, C., Bonnaire, N., Favez, O., Bonsang, B., and Gros, V.: Large contribution of water-insoluble secondary organic aerosols in the region of Paris (France) during wintertime, J. Geophys. Res.-Atmos., 116, D22203, https://doi.org/10.1029/2011JD015756, 2011.

Seibert, P., Kromp-Kolb, H., Baltensperger, U., Jost, D. T., Schwikowski, M., Kasper, A., and Puxbaum, H.: Trajectory analysis of aerosol measurements at high alpine sites, in: EUROTRAC Symposium 94, Garmish-Partenkirchen, Germany, Academic Publishing BV, the Hague, 1994.

Seinfeld, J. H. and Pandis, S. N.: Atmospheric Chemistry and Physics, Wiley-Interscience, New York, 1998.

Simpson, I. J., Akagi, S. K., Barletta, B., Blake, N. J., Choi, Y., Diskin, G. S., Fried, A., Fuelberg, H. E., Meinardi, S., Rowland, F. S., Vay, S. A., Weinheimer, A. J., Wennberg, P. O., Wiebring, P., Wisthaler, A., Yang, M., Yokelson, R. J., and Blake, D. R.: Boreal forest fire emissions in fresh Canadian smoke plumes: C_1–C_{10} volatile organic compounds (VOCs), CO_2, CO, NO_2, NO, HCN and CH_3CN, Atmos. Chem. Phys., 11, 6445–6463, https://doi.org/10.5194/acp-11-6445-2011, 2011.

Slowik, J. G., Vlasenko, A., McGuire, M., Evans, G. J., and Abbatt, J. P. D.: Simultaneous factor analysis of organic particle and gas mass spectra: AMS and PTR-MS measurements at an urban site, Atmos. Chem. Phys., 10, 1969–1988, https://doi.org/10.5194/acp-10-1969-2010, 2010.

Sorooshian, A., Brechtel, F. J., Ma, Y. L., Weber, R. J., Corless, A., Flagan, R. C., and Seinfeld, J. H.: Modeling and characterization of a particle-into-liquid sampler (PILS), Aerosol Sci. Tech., 40, 396–409, 2006.

Sorooshian, A., Lu, M. L., Brechtel, F. J., Jonsson, H., Feingold, G., Flagan, R. C., and Seinfeld, J. H., On the source of organic acid aerosol layers above clouds, Environ. Sci. Technol., 41, 4647–4654, 2007.

Stein, A., Draxler, R., Rolph, G., Stunder, B., Cohen, M., and Ngan, F.: NOAA's HYSPLIT atmospheric transport and dispersion modeling system, B. Am. Meteorol. Soc., 96, 2059–2077, https://doi.org/10.1175/BAMS-D-14-00110.1, 2015.

Stohl, A.: Trajectory statistics-a new method to establish source-receptor relationships of air pollutants and its application to the transport of particulate sulfate in Europe, Atmos. Environ., 30, 579–587, 1996.

Sullivan, A. P., Weber, R. J., Clements, A. L., Turner, J. R., Bae, M. S., and Schauer, J. J.: A method for on-line measurement of water-soluble organic carbon in ambient aerosol particles: Results from an urban site, Geophys. Res. Lett., 31, L13105, https://doi.org/10.1029/2004GL019681, 2004.

Sullivan, A. P., Peltier, R. E., Brock, C. A., de Gouw, J. A., Holloway, J. S., Warneke, C., Wollny, A. G., and Weber, R. J.: Airborne measurements of carbonaceous aerosol soluble in water over northeastern United States: Method development and an investigation into water-soluble organic carbon sources, J. Geo-phys. Res.-Atmos., 111, D23S46, https://doi.org/10.1029/2006JD007072, 2006.

Thunis, P., Triacchini, G., White, L., Maffeis, G., and Volta, V.: Air pollution and emission reductions over the Po-valley: Air Quality Modelling and Integrated Assessment, in: 18th world IMACS Congress and MODSIM09 International Congress on Modeling and Simulation, Interfacing Modeling and Simulation with Mathematical and Computational Sciences, Cairns, Australia from 13–17 July 2009, 2335–234, 2009.

Tian, Y. Z., Shi, G. L., Han, S. Q., Zhang, Y. F., Feng, Y. C., Liu, G. R., Gao, L. J., Wu, J. H., and Zhu, T.: Vertical characteristics of levels and potential sources of water-soluble ions in PM_{10} in a Chinese megacity, Sci. Total Environ., 447, 1–9, 2013.

Tyndall, G .S., Cox, R. A., Granier, C., Lesclaux, R., Moortgat, G. K., Pilling, M. J., Ravishankara, A. R., and Wallington, T. J.: Atmospheric chemistry of small organic peroxy radicals, J. Geophys. Res., 106, 12157–12182, 2001.

Ulbrich, I. M., Canagaratna, M. R., Zhang, Q., Worsnop, D. R., and Jimenez, J. L.: Interpretation of organic components from Positive Matrix Factorization of aerosol mass spectrometric data, Atmos. Chem. Phys., 9, 2891–2918, https://doi.org/10.5194/acp-9-2891-2009, 2009.

Vlasenko, A., Slowik, J. G., Bottenheim, J. W., Brickell, P. C., Chang, R. Y. W., Maedonald, A. M., Shantz, N. C., Sjostedt, S. J., Wiebe, H. A., Leaitch, W. R., and Abbatt, J. P. D.: Measurements of VOCs by proton transfer reaction mass spectrometry at a rural Ontario site: Sources and correlation to aerosol composition, J. Geophys. Res., 114, D21305, https://doi.org/10.1029/2009JD012025, 2009.

Volkamer, R., San Martini, F., Molina, L. T., Salcedo, D., Jimenez, J. L., and Molina, M. J.: A missing sink for gas-phase glyoxal in Mexico City: Formation of secondary organic aerosol, Geophys. Res. Let., 34, L19807, https://doi.org/10.1029/2007GL030752, 2007.

Warneck, P.: In-cloud chemistry opens pathway to the formation of oxalic acid in the marine atmosphere, Atmos. Environ., 37, 2423–2427, 2003.

Weber, R. J., Sullivan, A. P., Peltier, R. E., Russell, A., Yan, B., Zheng, M., de Gouw, J., Warneke, C., Brock, C., Holloway, J. S., Atlas, E. L., and Edgerton, E.: A study of secondary organic aerosol formation in the anthropogenic-influenced southeastern United States, J. Geophys. Res., 112, D13302, https://doi.org/10.1029/2007jd008408, 2007.

Wisthaler, A., Jensen, N. R., Winterhalter, R., Lindinger, W., and Hjorth, J.: Measurements of acetone and other gas phase product yields from the oh-initiated oxidation of terpenes by protontransfer-reaction mass spectrometry (ptr-ms), Atmos. Environ., 35, 6181–6191, 2001.

Yuan, B., Shao, M., de Gouw, J., Parrish, D. D., Lu, S., Wang, M., Zeng, L., Zhang, Q., Song, Y., Zhang, J., and Hu, M.: Volatile organic compounds (VOCs) in urban air: how chemistry affects the interpretation of positive matrix factorization (PMF) analysis, J. Geophys. Res., 117, D24302, 1–17, https://doi.org/10.1029/2012JD018236, 2012.

Zannoni, N., Dusanter, S., Gros, V., Sarda Esteve, R., Michoud, V., Sinha, V., Locoge, N., and Bonsang, B.: Intercomparison of two comparative reactivity method instruments inf the Mediterranean

basin during summer 2013, Atmos. Meas. Tech., 8, 3851–3865, https://doi.org/10.5194/amt-8-3851-2015, 2015.

Zannoni, N., Gros, V., Sarda Esteve, R., Kalogridis, C., Michoud, V., Dusanter, S., Sauvage, S., Locoge, N., Colomb, A., and Bonsang, B.: Summertime OH reactivity from a receptor coastal site in the Mediterranean basin, Atmos. Chem. Phys. Discuss., https://doi.org/10.5194/acp-2016-684, in review, 2016.

Zhang, Q., Jimenez, J., Canagaratna, M., Ulbrich, I., Ng, N., Worsnop, D., and Sun, Y.: Understanding atmospheric organic aerosols via factor analysis of aerosol mass spectrometry: a review, Anal. Bioanal. Chem., 401, 3045–3067, 2011.